A Mini Project Report

On

Brain Tumor Detection

By
K.RACHNA
17RH1A05A9

Under the Esteemed Guidance of

Mrs.K.MOUNIKA
Assistant Professor

in partial fulfillment of the Academic Requirements for the Degree of
BACHELOR OF TECHNOLOGY

Department of Computer Science and Engineering

MALLA REDDY ENGINEERING COLLEGE FOR WOMEN

(Autonomous Institution-UGC, Govt. of India)

Accredited by NBA & NAAC with 'A' Grade, UGC, Govt. of India
NIRF Indian Ranking, Accepted by MHRD, Govt. of India
Band A (6th to 25th) National Ranking by ARIIA, MHRD, Govt. of India
Approved by AICTE, ISO 9001:2015 Certified Institution
AAAA+ Rated by Digital Learning Magazine, AAA+ Rated by Careers 360 Magazine
3rd Rank CSR, Platinum Rated by AICTE-CII Survey, 141 National Ranking by India Today Magazine
National Ranking-Top 100 Rank band by Outlook Magazine, National Ranking-Top 100 Rank band by Times News Magazine
2020-2021

MALLA REDDY ENGINEERING COLLEGE FOR WOMEN
Accredited by NBA & NAAC with A-Grade

(Autonomous Institution-UGC, Govt. of India)
Accredited by NBA & NAAC with 'A' Grade, UGC, Govt. of India
NIRF Indian Ranking, Accepted by MHRD, Govt. of India
Band A (6th to 25th) National Ranking by ARIIA, MHRD, Govt. of India
Approved by AICTE, ISO 9001:2015 Certified Institution
AAAA+ Rated by Digital Learning Magazine, AAA+ Rated by Careers 360 Magazine
3rd Rank CSR, Platinum Rated by AICTE-CII Survey, 141 National Ranking by India Today Magazine
National Ranking-Top 100 Rank band by Outlook Magazine, National Ranking-Top 100 Rank band by Times News Magazine
2020-2021

Department of Computer Science and Engineering

DECLARATION

I hereby declare that the Mini Project entitled "**Brain Tumor Detection**" submitted to Malla Reddy Engineering College for Women affiliated to Jawaharlal Nehru Technological University, Hyderabad (JNTUH) for the award of the Degree of Bachelor of Technology in Computer Science and Engineering is result of original research work done by us. It is further declared that the Mini Project report or any part thereof has not been previously submitted to any University or Institute for the award of Degree.

RACHNA KOLA **(17RH1A05A9)**

MALLA REDDY ENGINEERING COLLEGE FOR WOMEN
Accredited by NBA & NAAC with A-Grade

(Autonomous Institution-UGC, Govt. of India)
Accredited by NBA & NAAC with 'A' Grade, UGC, Govt. of India
NIRF Indian Ranking, Accepted by MHRD, Govt. of India
Band A (6th to 25th) National Ranking by ARIIA, MHRD, Govt. of India
Approved by AICTE, ISO 9001:2015 Certified Institution
AAAA+ Rated by Digital Learning Magazine, AAA+ Rated by Careers 360 Magazine
3rd Rank CSR, Platinum Rated by AICTE-CII Survey, 141 National Ranking by India Today Magazine
National Ranking-Top 100 Rank band by Outlook Magazine, National Ranking-Top 100 Rank band by Times News Magazine
2020-2021

Department of Computer Science and Engineering

CERTIFICATE

This is to certify that the Mini Project work entitled **"Brain Tumor Detection"** submitted by

RACHNA KOLA (17RH1A05A9)

In partial fulfillment for the award of degree of **BACHELOR OF TECHNOLOGY** in Computer Science and Engineering, Jawaharlal Nehru Technological University, Hyderabad during the year **2020-2021.**

Project Guide	**Head of the Department**
Mrs.K.MOUNIKA **Assistant Professor**	**Dr. C.V.P.R.PRASAD** **Professor**

ABSTRACT

Image Segmentation is an important and challenging factor in the field of medical sciences. It is widely used for the detection of tumors. This paper deals with detection of brain tumor from MR images of the brain. The brain is the anterior most part of the nervous system. Tumor is a rapid uncontrolled growth of cells. Magnetic Resonance Imaging (MRI) is the device required to diagnose brain tumor. The normal MR images are not that suitable for fine analysis, so segmentation is an important process required for efficiently analyzing the tumor images. Clustering is suitable for biomedical image segmentation as it uses unsupervised learning. This paper work uses K-Means clustering where the detected tumor shows some abnormality which is then rectified by the use of morphological operators along with basic image processing techniques to meet the goal of separating the tumor cells from the normal cells.

ACKNOWLEDGEMENT

We feel ourselves honoured and privileged to place our warm salutation to our college Malla Reddy Engineering College for Women and Department of Computer Science and Engineering which gave us the opportunity to have expertise in engineering and profound technical knowledge.
We would like to deeply thank our Honourable Minister of Telangana State **Sri.Ch. MALLAREDDY Garu**, Founder Chairman MRGI, the largest cluster of institutions in the state of Telangana for providing us with all the resources in the college to make our project success.
We wish to convey gratitude to our Principal **Dr. Y. MADHAVEE LATHA**, for providing us with the environment and means to enrich our skills and motivating us in our endeavour and helping us to realize our full potential.
We would like to thank **Prof.A.RADHA RANI**, Director of Computer Science and Engineering & Information Technology for encouraging us to take up a project on this subject and motivating us towards the project work.
We express our sincere gratitude to **Dr. C.V.P.R.PRASAD**, Head of the Department of Computer Science and Engineering for inspiring us to take up a project on this subject and successfully guiding us towards its completion.
We would also like to thank our Project Co-Ordinator **Mr. KUMARASWAMY**, Assistant Professor for her kind encouragement and overall guidance in viewing this program a good asset with profound gratitude.
We would like to thank our Internal Guide **Mrs.K.MOUNIKA**, Assistant Professor and all the Faculty members for their valuable guidance and encouragement towards the completion of our project work.

With Regards & Gratitude,
RACHNA KOLA (17RH1A05A9)

Smart Internz

PROJECT COMPLETION CERTIFICATE

THIS CERTIFIES THAT

Rachna Kola

has successfully completed the project titled

“ Brain tumor detection from MRI images ”

with expected outcome.

APPROVEDB Y

TEAM SMARTINTERNZ

February 08, 2021

LIST OF FIGURES

INDEX

CHAPTER - 1
INTRODUCTION

Goal and Background

The goal of this project is to examine the effectiveness of symmetry features in detecting tumors in brain MRI scans.The normal human brain exhibits a high degree of symmetry. When a brain tumor is present, however, the brain becomes more asymmetric. Extracting symmetry features from the brain and training a classifier on these features should prove useful in locating tumors in the brain.This project is an extension of a project I have been working on this and last semester. The project involves detection of small and multiple tumors from the proposed dataset using blob detection. Tumors in the brain tend to be relatively compact and spherical a shape that in computer vision literature can be described as being blob-like.Thus, the cornerstone of the method I have used thus far is 3D blob detection. Using a 3D Laplacian of Gaussian filter, we generate a pool of blobs that become our initial tumor candidates and then prune them based on other features computed on these blobs. Among other features, the pruning has involved using a basic asymmetry feature that compares the histogram of each blob to its reflection-symmetrical counterpart blob. This feature, however, has not proven as discriminative as we would expect. I believe this is because, although the brain does exhibit a fair amount of symmetry from a large-scale perspective, it is fairly asymmetric when looking at the fine details of every voxel. A scale-space implementation of symmetry features is thus called for.

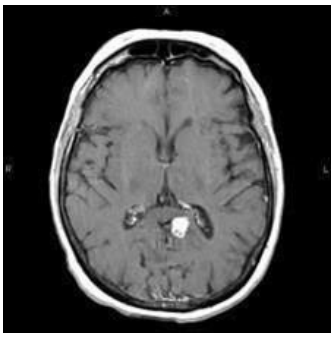

Dataset

The dataset used for this project consists of 20 patient MRI scans provided by Dr. Dan Nguyen

from the Milton S. Hershey Medical Center. These scans were obtained using a Phillips Intera 1.5 Tesla Magnet with a resolution of 231x185x200 pixels and 1mm slice thickness. They are T1 gadolinium-enhanced.

Each scan contains at least one tumor, with a maximum of 16 tumors in one case. There are 86 tumors in all, 2 - 38 mm in diameter (3 - 28,731 cubic mm volume). These include both primary and metastatic tumors of various sizes, some with dark necrotic cores. The ground truth, which involves the center and radius of each tumor, was given to us by Dr. Nguyen, the radiologist who provided the data.

The data has been pre-processed. It has been converted to ANALYZE format. Using fully automated midsagittal plane (MSP) extraction software , each scan was properly aligned. The skull and surrounding tissue were removed from the scans using FSL

CHAPTER - 2
The Method

Blob acquisition and Pruning

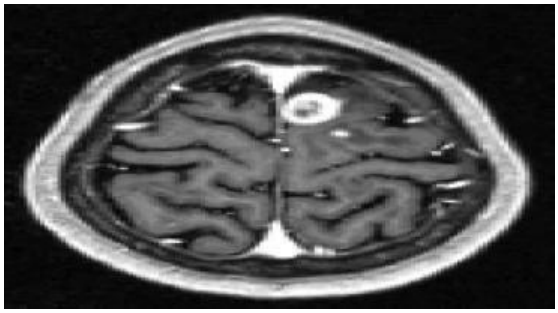

Fig. 1: Slice 136 of brain h38

We begin with an input volume that is centered and whose mid sagittal plane is aligned vertically (Fig. 1). Blobs are extracted from this brain using 3D Laplacian of Gaussian filters with varying sigma values, thus allowing us to find blobs of different sizes. The skull and surrounding tissue are not removed at this stage to allow maximum information to be used for blob detection. After filtering, a dilated brain mask is applied, allowing the border of the brain to be padded by true voxel intensities instead of a black background. This should make analysis more accurate.

At every voxel, the maximum achieved LoG value, along with the sigma associated with the filter from which this value was computed, are stored in one maximum LoG volume. Non-maximum suppression is then applied to every 5x5x5 non-zero box in this volume, keeping as a tumor candidate the voxel in each box with the highest LoG score. We record this voxel's coordinates along with the LoG score and the sigma value of the filter used to obtain this score. Fig. 2 shows the results of this non-maximum suppression.

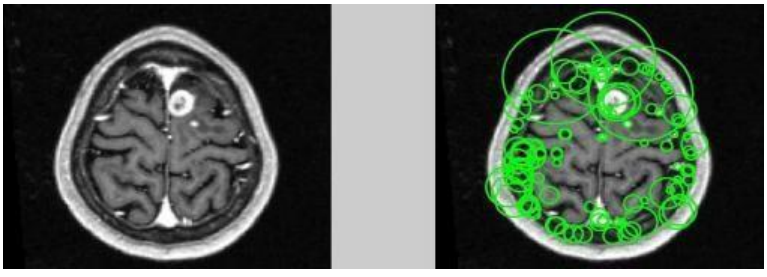

Fig. 2: The original volume and all the initial blobs after non-maximum suppression.

Following the initial blob detection, the blobs are pruned by a combination of three masks. The first, shown in Fig 3., is the brain-only mask obtained using FSL . This mask serves to remove all blobs outside the brain-only region.

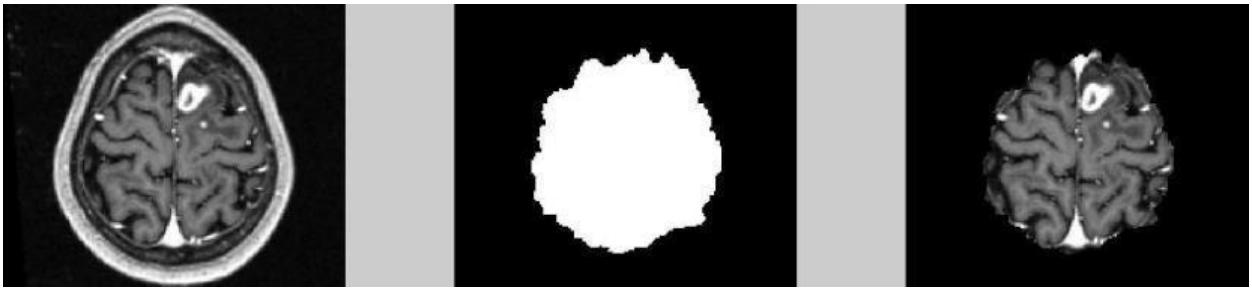

Fig 3. The original volume, the brain-only mask, and the brain mask applied to the original volume, respectively.

The second, shown in Fig. 4, takes into account deviations from the mean intensity, whether light or dark. Tumors are visually distinct from their surroundings, and this mask is meant to represent visual distinctiveness. It is obtained by finding the mean and standard deviation of the brain-only intensities (see rightmost image in Fig. 3) and subtracting the mean value from each brain-only voxel's intensity. The absolute value of these differences is then taken to account for voxels that are both lighter and darker than the mean. To create the mask, any voxels whose absolute difference from the mean is within one standard deviation of the mean are set to 0. All others are set to 1.

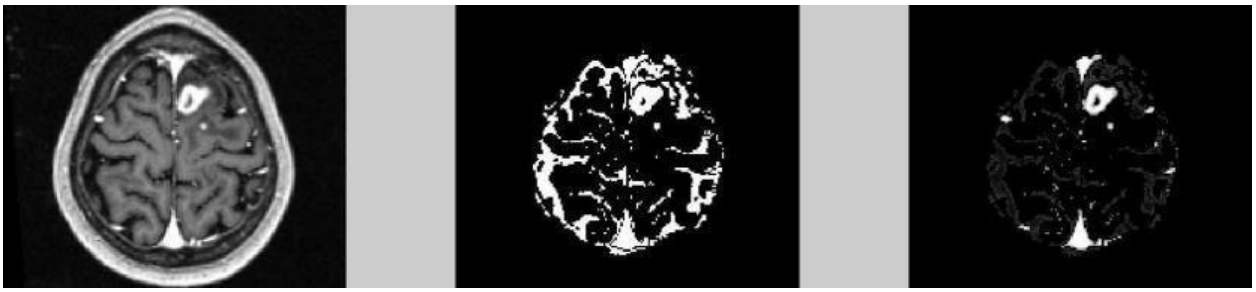

Fig 4. The original volume, the absolute intensity deviation mask, and the mask applied to the original volume, respectively.

The third mask, shown in Fig. 5, takes into account asymmetry. The brain-only portion of the original volume is reflected along the MSP. The absolute value of the difference between the brain-only portion of the original volume and the resulting image then forms the absolute difference image . To create the mask, any voxels where the absolute difference value is below 20% of the maximum value (20% of 255 = 51) are set to 0. All others are set to 1. To allow for blobs that are located along the MSP, which are self symmetric and thus would be pruned away by this mask, values along the MSP and 1 voxel to the right or left of it are set to 1.

Fig 5. The original volume, the asymmetry mask, and the mask applied to the original volume, respectively.

The three masks are combined (see Fig. 6) to form one mask that is used to perform the first pruning step.

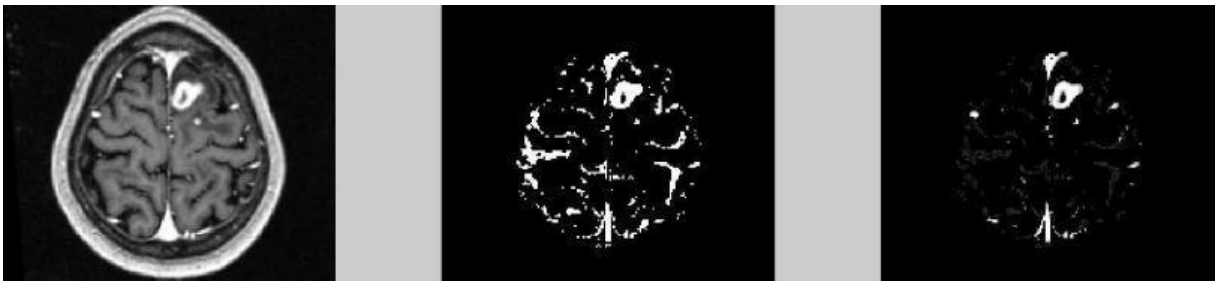

Fig 6. The original volume, the combined mask, and the mask applied to the original volume, respectively.

The combined mask is applied to the initial blobs and all blobs whose centers are located outside the mask are removed. The remaining blobs are significantly fewer in number (see Fig. 7 and Table 1).

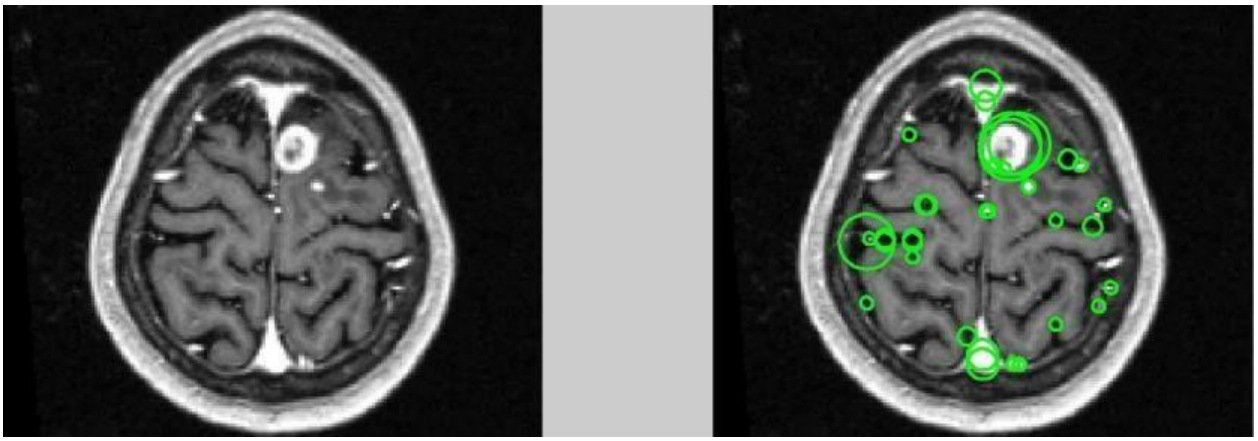

Fig 7. The original volume and the blobs remaining after the combined mask is applied.

The second pruning step removes blobs which are nearly symmetrical. Structures in the brain do not always line up perfectly across the MSP. Gliding along any direction may occur. To account for this, tolerated asymmetry pruning is performed as follows. Let *S* be the set of blobs that are remaining after mask pruning. Let *b* be a blob in *S*. We first locate the voxel, *vc*, that is the symmetrical counterpart of the center of *b*. We define a search area, *A*, that is a

21 x 21 x 21 box centered at v_C (allowing a movement of 10 voxels in each direction *x*, *y*, and *z*). Let S_b be the set of blobs in *S* whose centers are in *A*. If S_b is not empty, blob *b* is potentially symmetric. Further prune S_b by removing any blobs whose sigma value differs from *b*'s sigma value by more than 2, whose LoG score differs from *b*'s LoG score by more than 0.05, and whose mean intensity differs from *b*'s mean intensity by more than 10. If *b* is symmetric, the blobs that are symmetric to it should be of similar shape, blobbiness and intensity. If any blobs remain in S_b after this pruning, *b* is assumed symmetric and is removed, along with these blobs, from *S*. One exception is made if *b* is self-symmetric. In this case, *b* and any remaining blobs in S_b are kept since they are also likely self-symmetric. The blobs remaining after this second pruning step are shown in Fig. 8. The number of blobs pruned can be seen in Table 1.

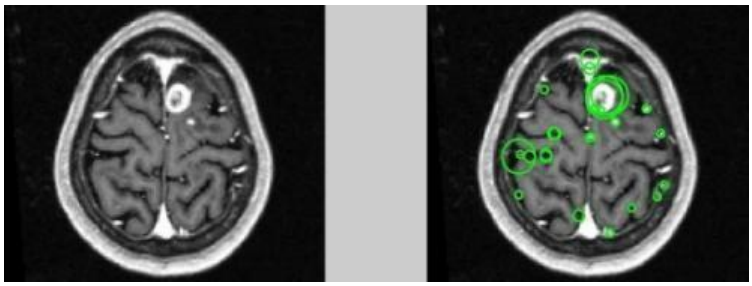

Fig 8. The original volume and the blobs remaining after nearlysymmetrical blobs are removed.

Case #	Initial Blobs	After Mask Pruning	After Tol. Asym. Pruning
1	16263	2905	1852
2	15389	3302	1510
3	16662	3593	2344
4	16287	2965	1659
5	17880	3608	2326
6	15225	2058	1386
7	15937	4171	2304
8	15317	3990	2653
9	14852	3535	1841
10	13676	3053	2118
11	14944	3274	1741
12	16295	3638	2079
13	18801	3268	2113
14	16984	3580	1615
15	17691	4222	2855
16	15950	3008	1515
17	18989	3911	1971
18	16849	4087	2247
19	15003	2964	1357
20	17513	3721	1880

Table 1. The number of blobs in each case after each pruning step. Case #18 corresponds to brain h38.

CHAPTER - 3
Feature Extraction
Usable features are extracted using seven volumes.

The volumes

The first volume is the original volume, masked by a dilated brain mask in order to keep the true voxel values at the edges of the brain (see Fig. 9).
The second volume is the absolute deviation volume (see Fig. 10). This is obtained the same way as the absolute intensity deviation mask but without thresholding. Thus, each value in this volume represents the absolute difference between the voxel's original intensity and the mean intensity of the brain-only voxels from the original volume.

The third volume is obtained by smoothing the original volume with a 3D Gaussian filter. For a blob with sigma value , features for this blob are computed using the volume that was smoothed by a 3D Gaussian filter with the same
This allows for features to be computed at the blob's own scale reducing "noise" from other scales. See Fig. 12 for all smoothed volumes. The fourth volume had been computed during the blob acquisition stage - the LoG volume. LoG volumes are obtained by filtering the original volume with 3D Laplacian of Gaussian filters with 1, 2, 3,...,16.

These same sigma values are used in smoothing and are the only sigma values that blobs may have. Once again, features computed for a blob with sigma value are obtained using the LoG volume that resulted from filtering with a LoG having the same. See Fig. 13 for all LoG volumes.

The next three images are the absolute difference images of the original volume (Fig. 11), the smoothed volumes (Fig. 14, 15), and the LoG volumes (Fig. 16,17), weighted by an intensity deviation prior, and are used as measures of asymmetry. The intensity deviation prior is simply the absolute deviation volume divided by its own maximum value, thus giving values between 0 and 1 at each voxel. It is used to offset the effects of taking the absolute value of the difference image. When a difference image is obtained, a bright asymmetric blob in the original volume will remain bright (although less so). A dark asymmetric blob in the original volume will have negative values. To give bright and dark blobs the same footing in the asymmetry image, an absolute value is taken. This, however, leads to symmetric asymmetry - the region opposite a light or dark asymmetric blob will have values that are the same as those of the blob, indicating the same degree of asymmetry.
Since we are only interested in the blob, this extra region needs to be removed. This is done by applying the prior, which gives more weight to the bright/dark blob and less to the normal brain tissue across the MSP from it.

Fig. 11

The absolute difference image of the original volume (left) and the same absolute difference image after the intensity deviation prior is applied (right). Only the weighted image was used for feature extraction.

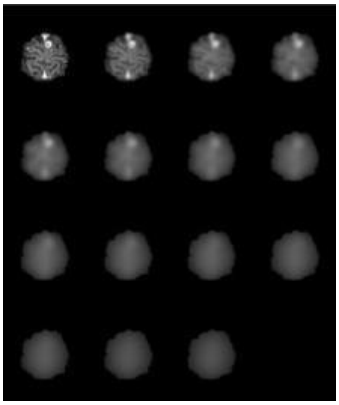

Fig. 12

The smoothed volumes obtained using Gaussian filters with increasing sigma values.

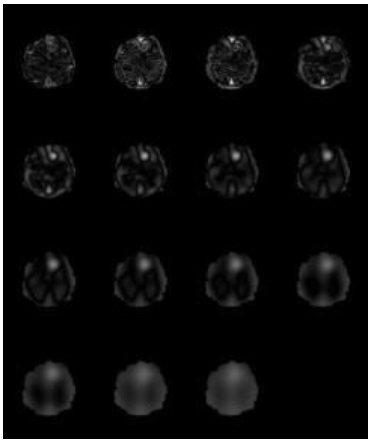

Fig. 13

The LoG volumes obtained using LoG filters with increasing sigma values. The LoG values in these images are rescaled to [0,255] to make feature extraction the same for each volume.

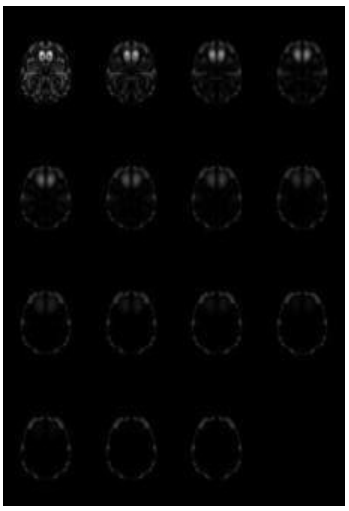

Fig. 14

The absolute difference images of the smoothed volumes obtained using Gaussian filters with increasing sigma values.

Note that these are nor weighted by the prior and hence are not used for feature extraction.

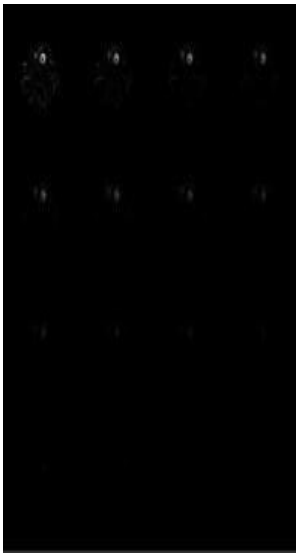

Fig. 15

The absolute difference images of the smoothed volumes obtained using Gaussian filters with increasing sigma values. Note that these are weighted by the prior and are the ones used for feature extraction.

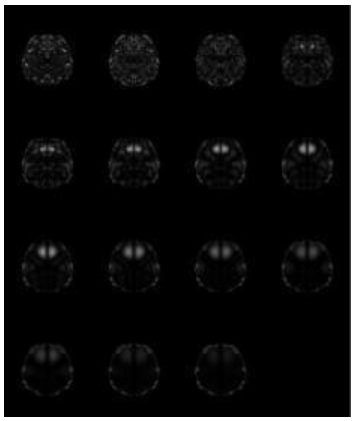

Fig. 16

The absolute difference images of the LoG volumes obtained using LoG filters with increasing sigma values. Note that these are nor weighted by the prior and hence are not used for feature extraction.

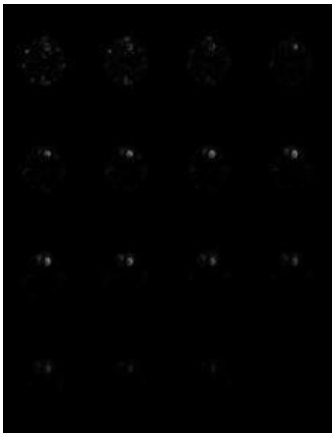

Fig. 17

The absolute difference images of the LoG volumes obtained using LoG filters with increasing sigma values.

Note that these are weighted by the prior and are the ones used for feature extraction.

Classification and Evaluation

The goal of this project was to test the efficacy of the new asymmetry features obtained. As much has changed over the course of this project, comparing current results to previous results would be unfair. The blobs are now obtained using 8 more scales, allowing for more granularity. They are also pruned by a combination of masks and filters that take into account more than just asymmetry. These differences make the dataset entering the classification step different from before. Because of this, I decided to test the feature effects on the new dataset only.

Preprocessing

Each blob was compared to the ground truth and received a label of tumor or non-tumor. To receive a label of tumor, the blob's center must be located within the volume of the ground truth tumor. The blobs from all brains are then pooled into one dataset. At the beginning of each experiment, the features of the training and testing datasets are normalized to [0,1] to avoid bias.

Data

Experiments were run on three different datasets. The first dataset only contained non-asymmetry features, which excludes the asymmetry feature and any features computed on difference images. The second dataset contained only asymmetry features - the asymmetry feature and those computed on the difference images. The final dataset used all 113 features.

Feature Selection

Because the feature set is small - there are only 113 features used - ranking is unnecessary; after normalization, the features are sent directly to Sequential Forward Selection (SFS). Two types of experiments were performed - using SFS wrapped around a QDA classifier, and using SFS wrapped around an LDA classifier. Both produced similar results.

Cross-Validation and Classification

Because there are more non-tumors than tumors, the split between training and testing data is determined by the tumors. 60% of the tumor data, and an equal number of non-tumor data is used for training. The remaining data is used for testing. Each time an experiment is run, the data is randomly split using this proportion. For cross-validation, each experiment is carried out 100 times and the classification results are averaged. LDA, QDA, Naive Bayes (Linear and Quadratic), SVM and a classifier using Mahalanobis distance were used.

Results

Results of these experiments and feature analysis can be seen in Appendix I.

CHAPTER - 4

Limitations, Issues, and Future Work

Ground Truth Confusion

Chen-Ping's ground truth

The student previously working on this project labeled the ground truth tumors. Unfortunately, some of the tumors were labeled in a way that made results better. For instance, if a blob was found on a tip of a tumor, that blob was recorded to be the ground truth, not the entire tumor. I decided to re-label the ground truth (see Appendix III for the most significant labeling changes). My ground truth tumors tend to overestimate the tumors, while Chen-Ping's underestimate. I also found a few large holes that were missed. Although they may not be tumors, they are abnormalities that our algorithm should still be picking up. The results with my ground truth are significantly worse than with Chen-Ping's ground truth (see Appendix II). I could not figure out why.

Labeling the blobs

My experiments from the mid-project report used data with a different labeling scheme than I am using right now. Before, for each ground truth tumor, I labeled as tumor the blob whose center was closest. I realized later that in reality, many blobs overlapped the ground truth tumor. My previous labeling would thus produce many blobs with similar characteristics but with only one labeled as tumor. I have now changed my labeling scheme to label any blob whose center is within a ground truth tumor as a tumor. The results are affected by this change and can be seen in Appendix IV.

More features

At some point during this project, I obtained features the same way but using voxels inside blobs with multiples of the true blobs' radii. Unfortunately, this led to dependency issues and created errors in my code that I did not have enough time to fix. While doing this, I experimented with redundancy removal techniques. One technique I had available to me was minimum Redundancy Maximum Relevance (mRMR), but the implementation required me to specify how many features it should return. Since there is no way to know how many features I should have, I decided to implement a different algorithm - FCBF. This algorithm first uses mutual information to find the most relevant features, then uses approximate Markov Blankets to find which features cover the information of which other features. This allows us to keep only the features that summarize the rest. This algorithm does not have a threshold if all features are first selected to be relevant.

Unfortunately, I was still getting errors and did not have time to figure out how to fix my code. This may be worthy of investigation later on.

Experimental Variables

Other feature selection methods can be used and wrapped around other classifiers. These are all variables that can be experimented with later on.

Final Feature Subset

I could not figure out how to construct a final "good" feature subset. Ideally, it would be the subset of features that appears in "most" of the runs. The size of this subset, as well as the definition of "most", are ill-defined.

Further Analysis

As the code is right now, it is difficult to analyze the blobs that were misclassified. Altering the code to allow this type of visualization would provide some insight into how to increase my rates. From a brief inspection of a handful of misclassified blobs, it appears that small bright structures in the brain are often easily confused for tumors.

CHAPTER - 5

Discussion and Conclusion

LDA vs. QDA

Wrapping SFS around LDA or QDA did not appear to make a significant difference in the results. I will thus discuss the results of the QDA-wrapped experiments. Also, Naive Bayes Linear and LDA, as well as Naive Bayes Quadratic and QDA, consistently have the same results. This is worth investigating further.

Efficiency of Asymmetry Features

It is difficult to compare my results now to those from my previous report. However, my new masks allowed me to reduce the total number of blobs going into the classification code from approximately 5,000 per brain to approximately 1,500-2,500 while keeping the classification rates the same. Thus, the masks' improvement is undeniable.

The symmetry features appear to have increased the mean sensitivity rates by ~1.5% and the mean specificity rates by ~2.3%. 2.3% increase in specificity means 175.74 more of the 37,641 non-tumor blobs were classified correctly. QDA had the best specificity, while LDA had the best sensitivity. Taking the total testing false positives achieved by QDA and dividing by 8 (since 40% of the 20 brains were used for testing), the final per-brain false positive count is approximately 218.7, down from 325.41. The same calculation done on LDA results yields 294.3 false positives per brain, down from 401.89. Although these numbers are high, they can be reduced by further pruning. For instance, right now, many blobs overlap each other and can be removed as redundant.

Regarding the feature selection - the results don't have clear winners. Asymmetry-EMD and compactness features computed on the LoG volume appear in nearly every run of the experiment. However, other statistics, such as std, max and skewness of the LoG volume are chosen the least. The original volume, besides in compactness, is usually less chosen than other volumes for a given feature. Many features are selected very frequently, so it is hard to do analysis. The length of the average selected feature subset is 87 out of 113. This implies that most of the features work together. Analysis may be easier if the features are grouped into categories. Frequency of category selection may yield more insight into the feature selection problem.

Comparison to State-of-the-Art

Two state-of-the-art papers do similar classification. My results are much better than those of, which achieves 90% sensitivity at the cost of 1600-1800 false positives per head. My results are somewhat comparable to those of an 89.9% sensitivity is achieved with approximately 34.8 false positives per head. My sensitivity is higher - 96% - at the cost of 8.5 times the false positives per head - 294.3. provides an in-depth analysis of tumor types and gives rates for each type. This can be interesting to compare. Because our datasets are different, however, a true comparison is infeasible.

UML DIAGRAMS

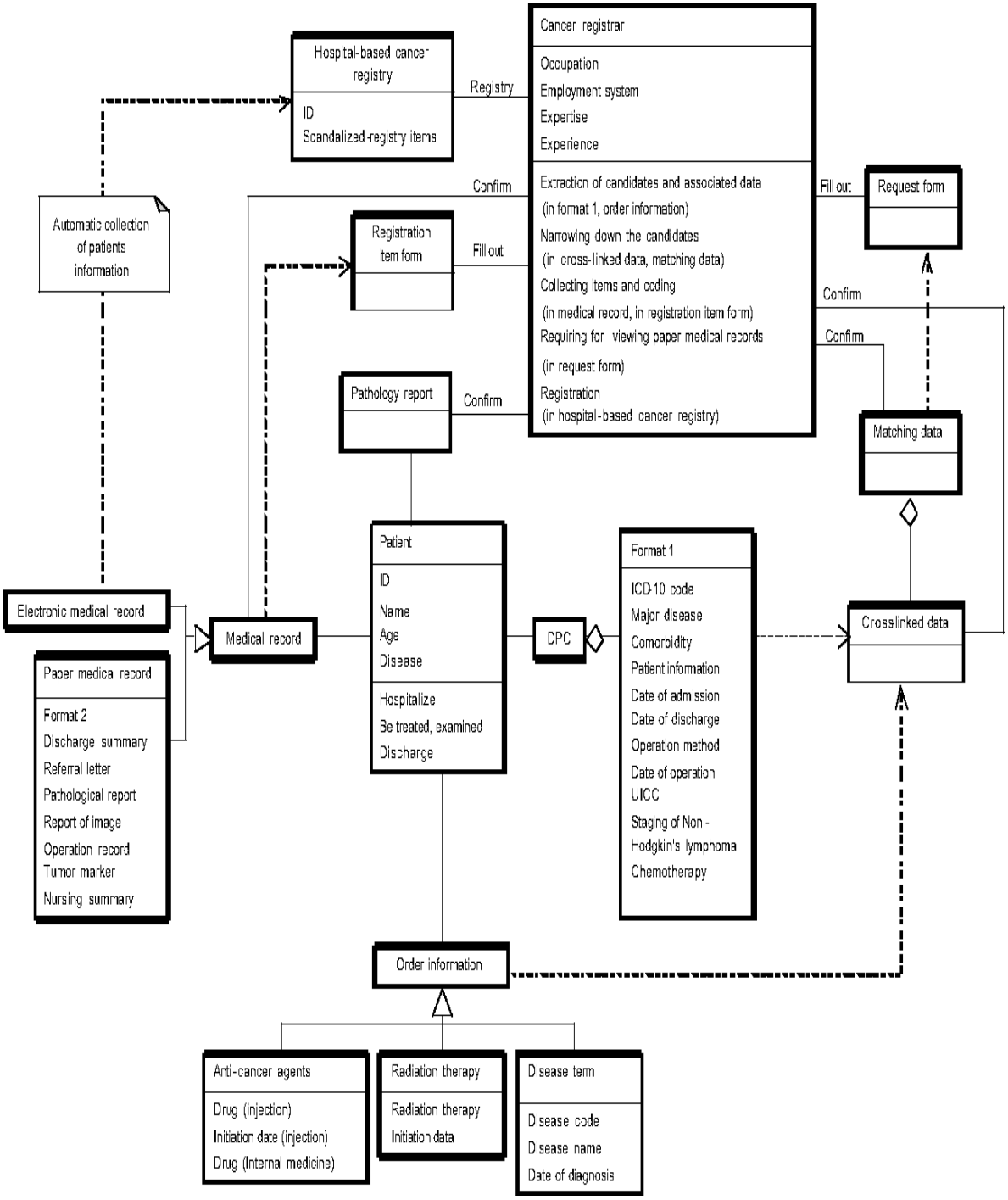

Fig: Activity Diagram

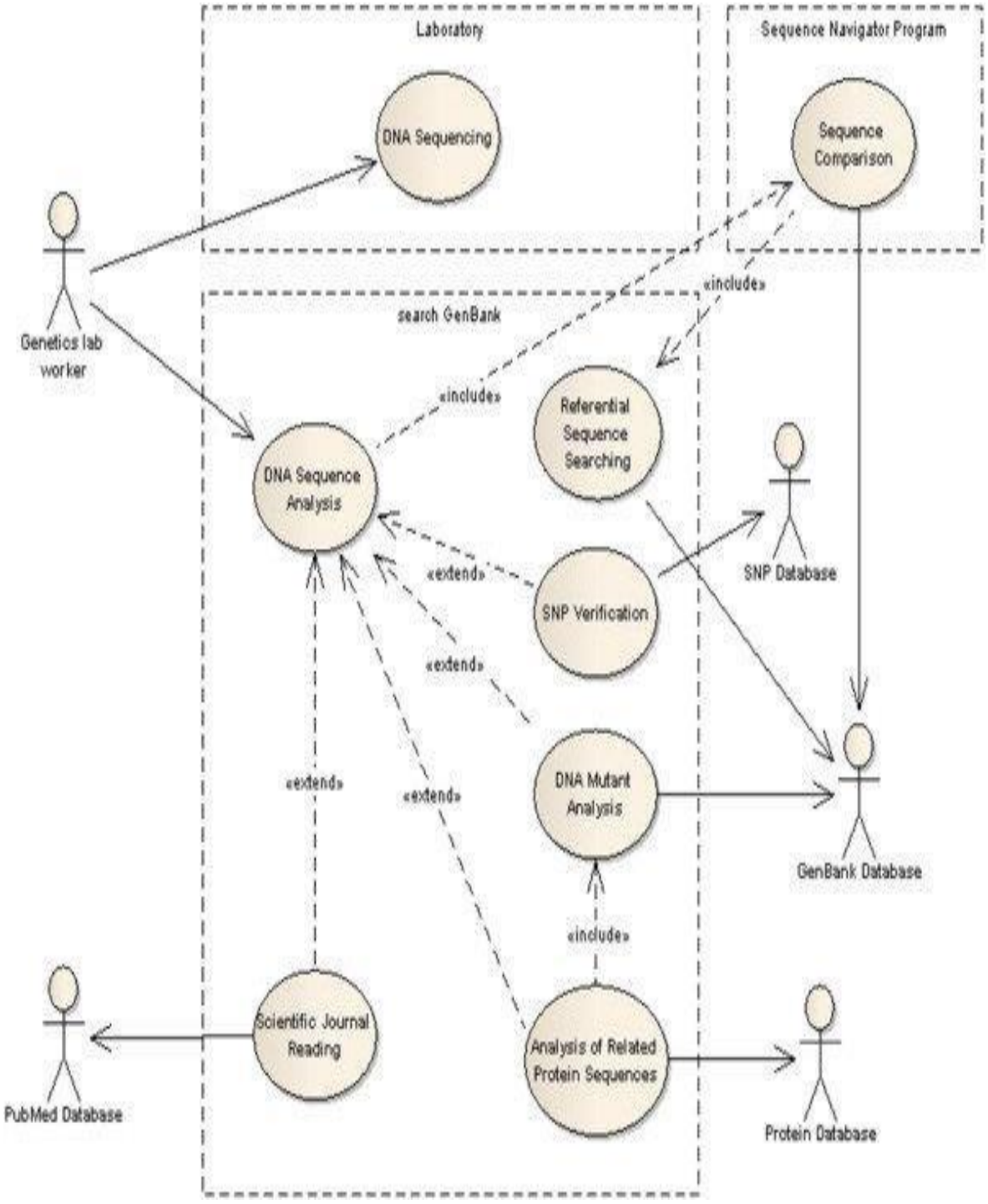

Fig. Use Case Diagram

CHAPTER – 6 (i)

Charts and Tables - Classification Results

A. No Asymmetry Features - SFS with QDA

Classifier	Tumor (Sensitivity)		Non-Tumor (Specificity)		Overall	
	Training	Test	Training	Test	Training	Test
Mahalabonis	93.4(+-0.6)	92.6(+-1.3)	94.9(+-0.7)	93.8(+-0.5)	94.2(+-0.5)	93.8(+-0.5)
Bayes(Lin)	95.1(+-0.7)	94.4(+-1.1)	92.5(+-0.8)	91.4(+-0.7)	93.8(+-0.5)	91.4(+-0.7)
Bayes(Quad)	94.5(+-0.6)	93.2(+-1.3)	94.6(+-0.7)	93.0(+-0.6)	94.5(+-0.5)	93.0(+-0.6)
LDA	95.1(+-0.7)	94.4(+-1.1)	92.5(+-0.8)	91.4(+-0.7)	93.8(+-0.5)	91.4(+-0.7)
QDA	94.5(+-0.6)	93.2(+-1.3)	94.6(+-0.7)	93.0(+-0.6)	94.5(+-0.5)	93.0(+-0.6)
SVM (linear)	91.0(+-1.1)	90.6(+-1.7)	88.6(+-1.8)	88.2(+-1.7)	89.8(+-1.0)	88.3(+-1.7)

No Asymmetry Features - SFS with LDA

Classifier	Tumor (Sensitivity)		Non-Tumor (Specificity)		Overall	
	Training	Test	Training	Test	Training	Test
Mahalabonis	93.1(+-0.5)	92.5(+-1.3)	94.5(+-0.6)	93.8(+-0.6)	93.8(+-0.5)	93.8(+-0.5)
Bayes(Lin)	95.5(+-0.7)	94.4(+-1.2)	93.1(+-0.7)	91.5(+-0.6)	94.3(+-0.4)	91.5(+-0.6)
Bayes(Quad)	93.9(+-0.6)	93.2(+-1.3)	94.0(+-0.6)	93.1(+-0.6)	93.9(+-0.5)	93.1(+-0.5)
LDA	95.5(+-0.7)	94.4(+-1.2)	93.1(+-0.7)	91.5(+-0.6)	94.3(+-0.4)	91.5(+-0.6)
QDA	93.9(+-0.6)	93.2(+-1.3)	94.0(+-0.6)	93.1(+-0.6)	93.9(+-0.5)	93.1(+-0.5)
SVM (linear)	90.9(+-1.0)	90.7(+-1.8)	88.7(+-1.9)	88.3(+-1.7)	89.8(+-1.1)	88.3(+-1.7)

B. Only Asymmetry Features - SFS with QDA

Classifier	Tumor (Sensitivity)		Non-Tumor (Specificity)		Overall	
	Training	Test	Training	Test	Training	Test
Mahalabonis	92.5(+-0.6)	91.7(+-1.3)	93.6(+-0.8)	92.5(+-0.6)	93.1(+-0.6)	92.4(+-0.6)
Bayes(Lin)	93.4(+-0.7)	92.6(+-1.2)	92.3(+-0.9)	91.2(+-0.5)	92.9(+-0.6)	91.2(+-0.5)
Bayes(Quad)	93.2(+-0.6)	92.1(+-1.2)	93.4(+-0.8)	91.9(+-0.5)	93.3(+-0.6)	91.9(+-0.5)
LDA	93.4(+-0.7)	92.6(+-1.2)	92.3(+-0.9)	91.2(+-0.5)	92.9(+-0.6)	91.2(+-0.5)
QDA	93.2(+-0.6)	92.1(+-1.2)	93.4(+-0.8)	91.9(+-0.5)	93.3(+-0.6)	91.9(+-0.5)
SVM (linear)	88.3(+-1.4)	87.9(+-1.9)	88.7(+-1.5)	88.5(+-1.3)	88.5(+-1.1)	88.5(+-1.3)

Only Asymmetry Features - SFS with LDA

Classifier	Tumor (Sensitivity)		Non-Tumor (Specificity)		Overall	
	Training	Test	Training	Test	Training	Test
Mahalabonis	92.4(+-0.6)	91.6(+-1.4)	93.5(+-0.8)	92.3(+-0.5)	92.9(+-0.5)	92.3(+-0.5)
Bayes(Lin)	93.5(+-0.7)	92.5(+-1.3)	92.8(+-0.9)	91.1(+-0.5)	93.2(+-0.5)	91.1(+-0.5)
Bayes(Quad)	92.9(+-0.6)	92.1(+-1.3)	93.1(+-0.8)	91.8(+-0.5)	93.0(+-0.6)	91.8(+-0.5)
LDA	93.5(+-0.7)	92.5(+-1.3)	92.8(+-0.9)	91.1(+-0.5)	93.2(+-0.5)	91.1(+-0.5)
QDA	92.9(+-0.6)	92.1(+-1.3)	93.1(+-0.8)	91.8(+-0.5)	93.0(+-0.6)	91.8(+-0.5)
SVM (linear)	88.0(+-1.8)	87.7(+-2.1)	88.7(+-1.4)	88.4(+-1.4)	88.3(+-1.3)	88.3(+-1.3)

C. All Features - SFS with QDA

Classifier	Tumor (Sensitivity)		Non-Tumor (Specificity)		Overall	
	Training	Test	Training	Test	Training	Test
Mahalabonis	95.6(+-0.5)	94.2(+-1.2)	97.2(+-0.6)	95.7(+-0.4)	96.4(+-0.4)	95.7(+-0.4)
Bayes(Lin)	97.1(+-0.4)	96.0(+-1.0)	95.1(+-0.8)	93.7(+-0.6)	96.1(+-0.4)	93.7(+-0.6)
Bayes(Quad)	96.5(+-0.4)	94.6(+-1.1)	97.1(+-0.5)	95.3(+-0.4)	96.8(+-0.4)	95.3(+-0.4)
LDA	97.1(+-0.4)	96.0(+-1.0)	95.1(+-0.8)	93.7(+-0.6)	96.1(+-0.4)	93.7(+-0.6)
QDA	96.5(+-0.4)	94.6(+-1.1)	97.1(+-0.5)	95.3(+-0.4)	96.8(+-0.4)	95.3(+-0.4)
SVM (linear)	91.8(+-1.2)	91.5(+-1.5)	90.4(+-1.4)	90.0(+-1.2)	91.1(+-1.0)	90.1(+-1.2)

All Features - SFS with LDA

Classifier	Tumor (Sensitivity)		Non-Tumor (Specificity)		Overall	
	Training	Test	Training	Test	Training	Test
Mahalabonis	95.1(+-0.6)	94.2(+-1.1)	96.9(+-0.6)	95.7(+-0.4)	96.0(+-0.5)	95.7(+-0.4)
Bayes(Lin)	97.5(+-0.4)	96.0(+-0.8)	96.1(+-0.7)	93.8(+-0.5)	96.8(+-0.4)	93.8(+-0.5)
Bayes(Quad)	95.7(+-0.5)	94.8(+-1.0)	96.6(+-0.6)	95.3(+-0.4)	96.2(+-0.5)	95.3(+-0.4)
LDA	97.5(+-0.4)	96.0(+-0.8)	96.1(+-0.7)	93.8(+-0.5)	96.8(+-0.4)	93.8(+-0.5)
QDA	95.7(+-0.5)	94.8(+-1.0)	96.6(+-0.6)	95.3(+-0.4)	96.2(+-0.5)	95.3(+-0.4)
SVM (linear)	91.7(+-1.2)	91.5(+-1.6)	90.2(+-1.7)	89.9(+-1.5)	91.0(+-1.0)	89.9(+-1.4)

Charts and Tables - Confusion Matrices

A. No Asymmetry Features - SFS with QDA

confusion matrix Training set : Total Tumors :647 ; Total Non-Tumors :647 ; Test set : Total Tumors :431 ; Total Non-Tumors :37641;							
TT (True Positive)		TN (False Positive)		NT (False Negative)		NN (True Negative)	
Training	Test	Training	Test	Training	Test	Training	Test
604.6(+-3.9)	399.2(+-5.9)	32.6(+-4.8)	2322.4(+-217.4)	42.3(+-3.9)	31.7(+-5.9)	614.3(+-4.8)	35318.5(+-217.4)
615.8(+-5.0)	407.1(+-4.8)	48.2(+-5.7)	3215.1(+-285.1)	31.1(+-5.0)	23.8(+-4.8)	598.7(+-5.7)	34425.8(+-285.1)
611.5(+-4.0)	402.0(+-5.6)	34.4(+-4.9)	2603.3(+-233.6)	35.4(+-4.0)	28.9(+-5.6)	612.5(+-4.9)	35037.6(+-233.6)
615.8(+-5.0)	407.1(+-4.8)	48.2(+-5.7)	3215.1(+-285.1)	31.1(+-5.0)	23.8(+-4.8)	598.7(+-5.7)	34425.8(+-285.1)
611.5(+-4.0)	402.0(+-5.6)	34.4(+-4.9)	2603.3(+-233.6)	35.4(+-4.0)	28.9(+-5.6)	612.5(+-4.9)	35037.6(+-233.6)
589.2(+-7.5)	390.7(+-7.5)	73.6(+-12.2)	4413.9(+-659.9)	57.7(+-7.5)	40.3(+-7.5)	573.3(+-12.2)	33227.0(+-659.9)

No Asymmetry Features - SFS with LDA

confusion matrix Training set : Total Tumors :647 ; Total Non-Tumors :647 ; Test set : Total Tumors :431 ; Total Non-Tumors :37641;							
TT (True Positive)		TN (False Positive)		NT (False Negative)		NN (True Negative)	
Training	Test	Training	Test	Training	Test	Training	Test
602.3(+-3.8)	398.9(+-6.0)	35.0(+-4.4)	2323.8(+-226.9)	44.6(+-3.8)	32.1(+-6.0)	611.9(+-4.4)	35317.1(+-226.9)
618.3(+-4.5)	407.2(+-5.3)	44.0(+-4.6)	3192.3(+-251.5)	28.6(+-4.5)	23.7(+-5.3)	602.9(+-4.6)	34448.6(+-251.5)
607.5(+-3.9)	402(+-5.7)	38.6(+-4.3)	2597.3(+-228.6)	39.4(+-3.9)	29(+-5.7)	608.3(+-4.3)	35043.6(+-228.6)
618.3(+-4.5)	407.2(+-5.3)	44.0(+-4.6)	3192.3(+-251.5)	28.6(+-4.5)	23.7(+-5.3)	602.9(+-4.6)	34448.6(+-251.5)
607.5(+-3.9)	402(+-5.7)	38.6(+-4.3)	2597.3(+-228.6)	39.4(+-3.9)	29(+-5.7)	608.3(+-4.3)	35043.6(+-228.6)
588.7(+-7.0)	391.0(+-8.0)	72.6(+-12.6)	4390.9(+-668.5)	58.3(+-7.0)	39.9(+-8.0)	574.3(+-12.6)	33250.0(+-668.5)

B. Only Asymmetry Features - SFS with QDA

confusion matrix Training set : Total Tumors :647 ; Total Non-Tumors :647 ; Test set : Total Tumors :431 ; Total Non-Tumors :37641;							
TT (True Positive)		TN (False Positive)		NT (False Negative)		NN (True Negative)	
Training	Test	Training	Test	Training	Test	Training	Test
598.8(+-4.3)	395.4(+-5.9)	40.8(+-5.3)	2820.0(+-245.0)	48.1(+-4.3)	35.5(+-5.9)	606.1(+-5.3)	34820.9(+-245.0)
604.6(+-4.8)	399.3(+-5.1)	49.4(+-6.3)	3311.0(+-216.0)	42.4(+-4.8)	31.6(+-5.1)	597.5(+-6.3)	34329.9(+-216.0)
603.0(+-4.4)	397.2(+-5.5)	42.3(+-5.4)	3019.6(+-223.8)	43.9(+-4.4)	33.7(+-5.5)	604.6(+-5.4)	34621.3(+-223.8)
604.6(+-4.8)	399.3(+-5.1)	49.4(+-6.3)	3311.0(+-216.0)	42.4(+-4.8)	31.6(+-5.1)	597.5(+-6.3)	34329.9(+-216.0)
603.0(+-4.4)	397.2(+-5.5)	42.3(+-5.4)	3019.6(+-223.8)	43.9(+-4.4)	33.7(+-5.5)	604.6(+-5.4)	34621.3(+-223.8)
571.7(+-9.3)	379.1(+-8.2)	72.6(+-10.0)	4302.0(+-520.3)	75.2(+-9.3)	51.8(+-8.2)	574.3(+-10.0)	33338.9(+-520.3)

Only Asymmetry Features - SFS with LDA

confusion matrix Training set : Total Tumors :647 ; Total Non-Tumors :647 ; Test set : Total Tumors :431 ; Total Non-Tumors :37641;							
TT (True Positive)		TN (False Positive)		NT (False Negative)		NN (True Negative)	
Training	Test	Training	Test	Training	Test	Training	Test
598.0(+-4.1)	395(+-6.2)	41.9(+-5.2)	2863.5(+-214.6)	48.9(+-4.1)	36(+-6.2)	605.0(+-5.2)	34777.4(+-214.6)
605.4(+-4.8)	399.0(+-5.7)	46.2(+-6.0)	3325.1(+-215.6)	41.5(+-4.8)	31.9(+-5.7)	600.7(+-6.0)	34315.8(+-215.6)
601.1(+-4.2)	396.9(+-5.9)	44.0(+-5.7)	3056.2(+-202.5)	45.8(+-4.2)	34.0(+-5.9)	602.9(+-5.7)	34584.7(+-202.5)
605.4(+-4.8)	399.0(+-5.7)	46.2(+-6.0)	3325.1(+-215.6)	41.5(+-4.8)	31.9(+-5.7)	600.7(+-6.0)	34315.8(+-215.6)
601.1(+-4.2)	396.9(+-5.9)	44.0(+-5.7)	3056.2(+-202.5)	45.8(+-4.2)	34.0(+-5.9)	602.9(+-5.7)	34584.7(+-202.5)
569.5(+-11.9)	378.3(+-9.2)	72.8(+-9.5)	4364.9(+-531.2)	77.4(+-11.9)	52.7(+-9.2)	574.1(+-9.5)	33276.0(+-531.2)

C. All Features - SFS with QDA

confusion matrix Training set : Total Tumors :647 ; Total Non-Tumors :647 ; Test set : Total Tumors :431 ; Total Non-Tumors :37641;							
TT (True Positive)		TN (False Positive)		NT (False Negative)		NN (True Negative)	
Training	Test	Training	Test	Training	Test	Training	Test
618.7(+-3.6)	406.1(+-5.1)	17.7(+-3.9)	1585.4(+-173.5)	28.2(+-3.6)	24.8(+-5.1)	629.2(+-3.9)	36055.6(+-173.5)
628.3(+-3.0)	413.9(+-4.4)	31.3(+-5.6)	2354.4(+-236.1)	18.6(+-3.0)	17.0(+-4.4)	615.6(+-5.6)	35286.5(+-236.1)
624.8(+-3.1)	408.1(+-4.9)	18.5(+-3.8)	1749.5(+-184.8)	22.1(+-3.1)	22.8(+-4.9)	628.4(+-3.8)	35891.4(+-184.8)
628.3(+-3.0)	413.9(+-4.4)	31.3(+-5.6)	2354.4(+-236.1)	18.6(+-3.0)	17.0(+-4.4)	615.6(+-5.6)	35286.5(+-236.1)
624.8(+-3.1)	408.1(+-4.9)	18.5(+-3.8)	1749.5(+-184.8)	22.1(+-3.1)	22.8(+-4.9)	628.4(+-3.8)	35891.4(+-184.8)
594.4(+-8.2)	394.3(+-6.5)	62.0(+-9.4)	3728.5(+-476.1)	52.5(+-8.2)	36.6(+-6.5)	584.9(+-9.4)	33912.4(+-476.1)

All Features - SFS with LDA

confusion matrix Training set : Total Tumors :647 ; Total Non-Tumors :647 ; Test set : Total Tumors :431 ; Total Non-Tumors :37641;							
TT (True Positive)		TN (False Positive)		NT (False Negative)		NN (True Negative)	
Training	Test	Training	Test	Training	Test	Training	Test
615.9(+-3.9)	406.3(+-5.1)	20.0(+-4.3)	1593.5(+-166.3)	31.0(+-3.9)	24.6(+-5.1)	626.9(+-4.3)	36047.4(+-166.3)
630.9(+-3.0)	414.1(+-3.6)	25.1(+-4.7)	2323.6(+-192.9)	16.0(+-3.0)	16.8(+-3.6)	621.8(+-4.7)	35317.3(+-192.9)
619.5(+-3.7)	408.6(+-4.4)	21.6(+-4.5)	1748.3(+-173.2)	27.4(+-3.7)	22.3(+-4.4)	625.3(+-4.5)	35892.6(+-173.2)
630.9(+-3.0)	414.1(+-3.6)	25.1(+-4.7)	2323.6(+-192.9)	16.0(+-3.0)	16.8(+-3.6)	621.8(+-4.7)	35317.3(+-192.9)
619.5(+-3.7)	408.6(+-4.4)	21.6(+-4.5)	1748.3(+-173.2)	27.4(+-3.7)	22.3(+-4.4)	625.3(+-4.5)	35892.6(+-173.2)
593.3(+-7.9)	394.7(+-7.0)	62.8(+-11.1)	3793.4(+-569.4)	53.6(+-7.9)	36.2(+-7.0)	584.1(+-11.1)	33847.5(+-569.4)

Charts and Tables - Feature Selection Histograms

A. No Asymmetry Features - SFS with QDA (46.97 +- 7.0187 out of 61)

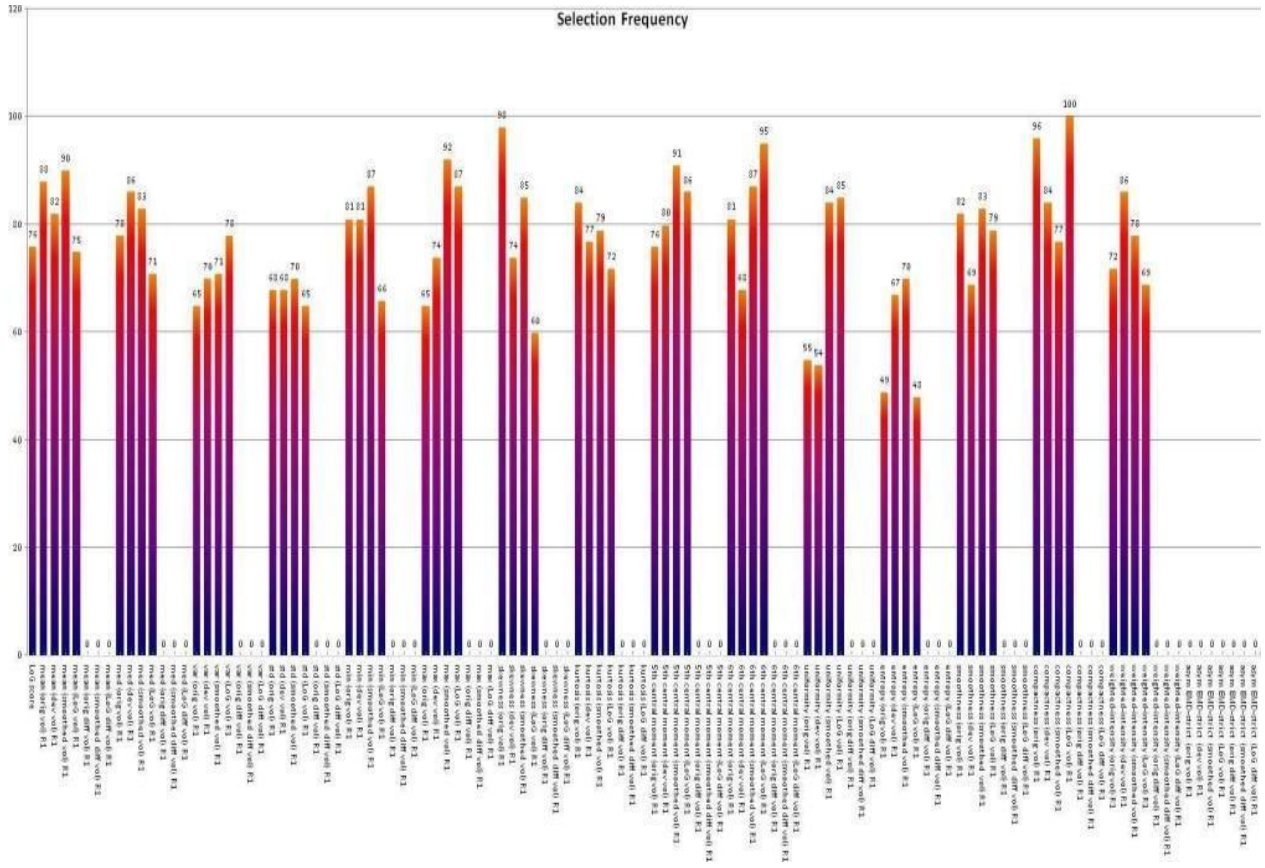

No Asymmetry Features - SFS with LDA (46.39 +- 7.3084 out of 61)

A. Only Asymmetry Features - SFS with QDA (41.58 +- 5.9479 out of52)

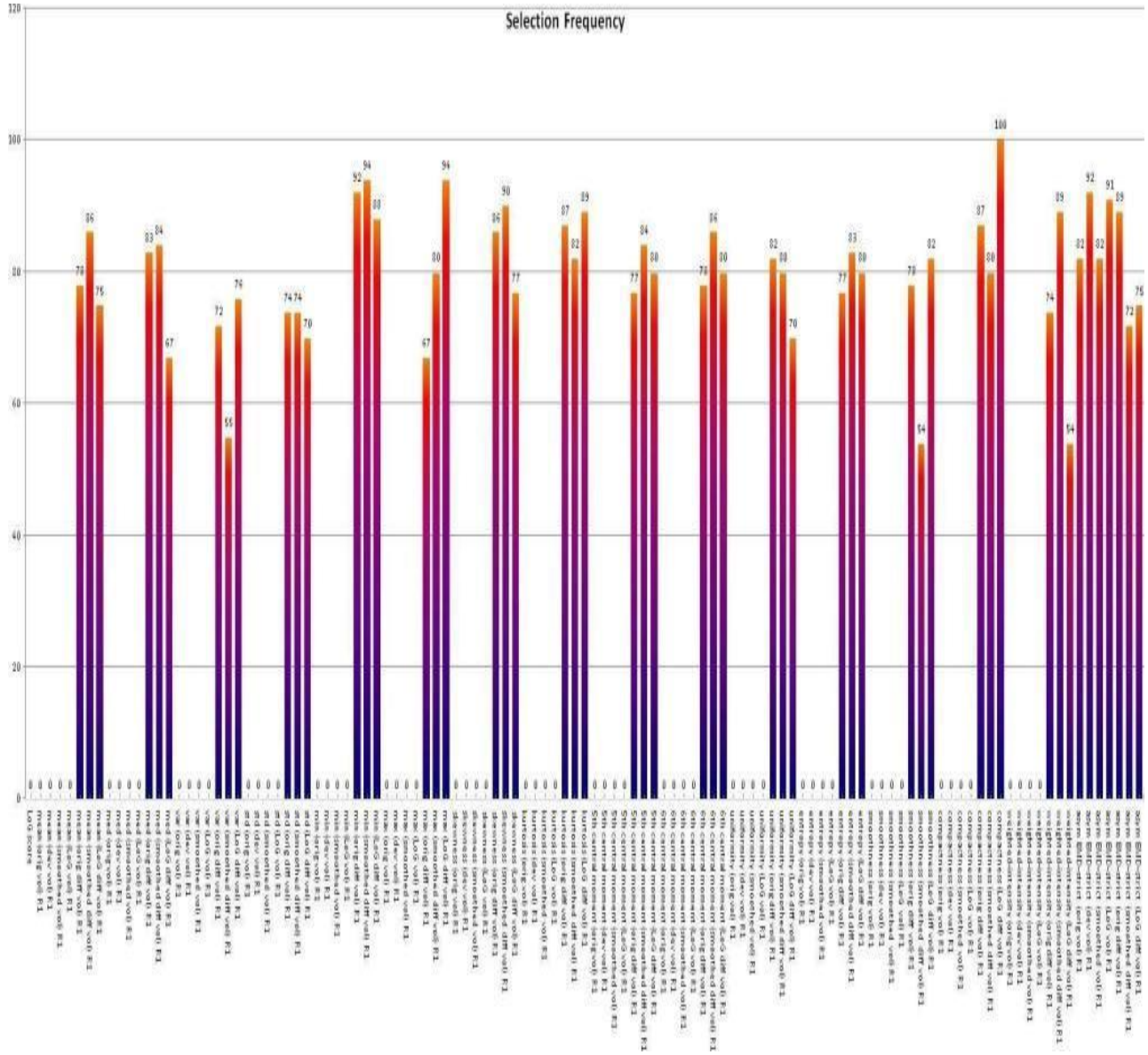

B. All Features - SFS with QDA (87.13 +- 15.03 out of 113)

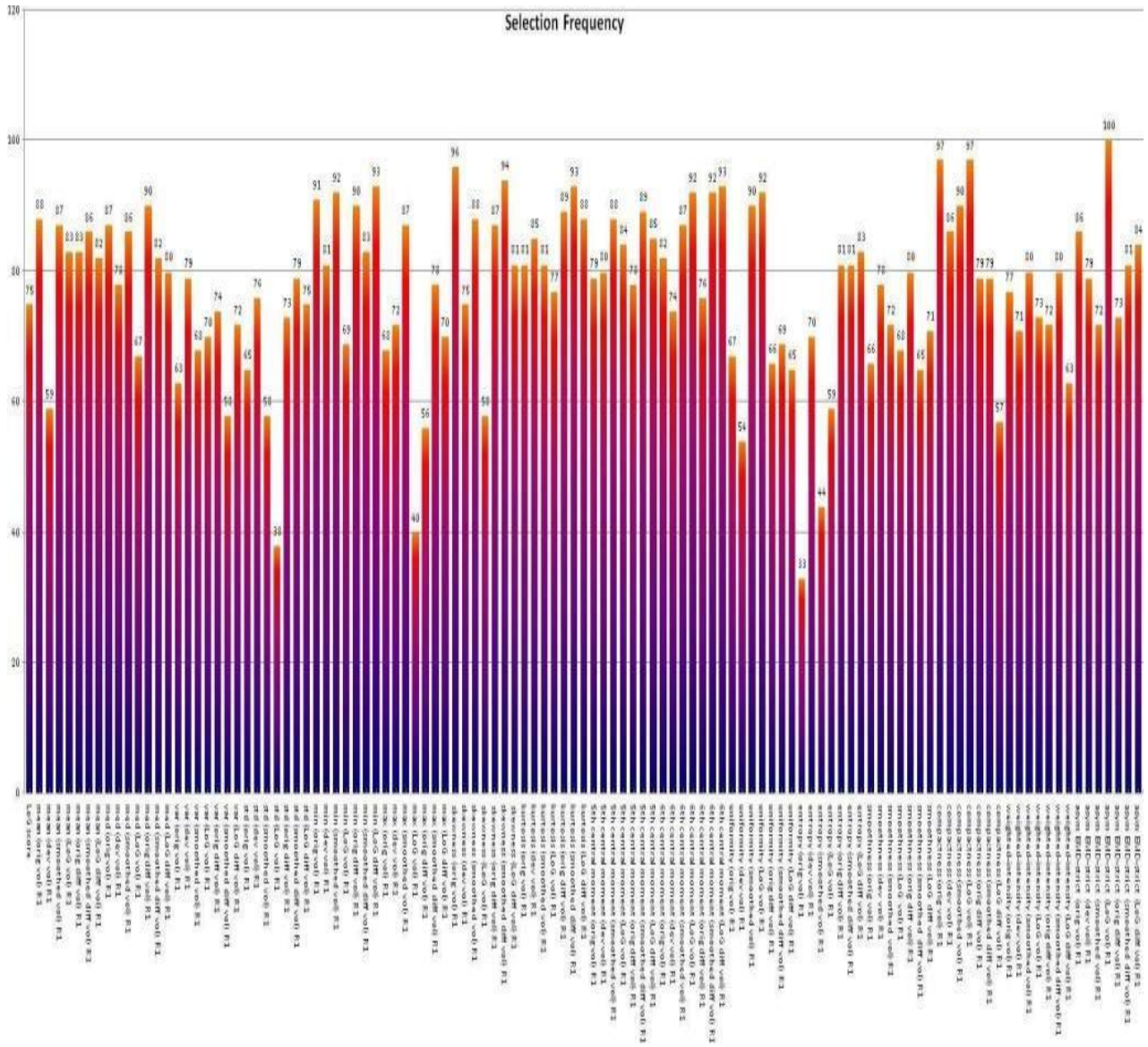

AVR Scores For All Features

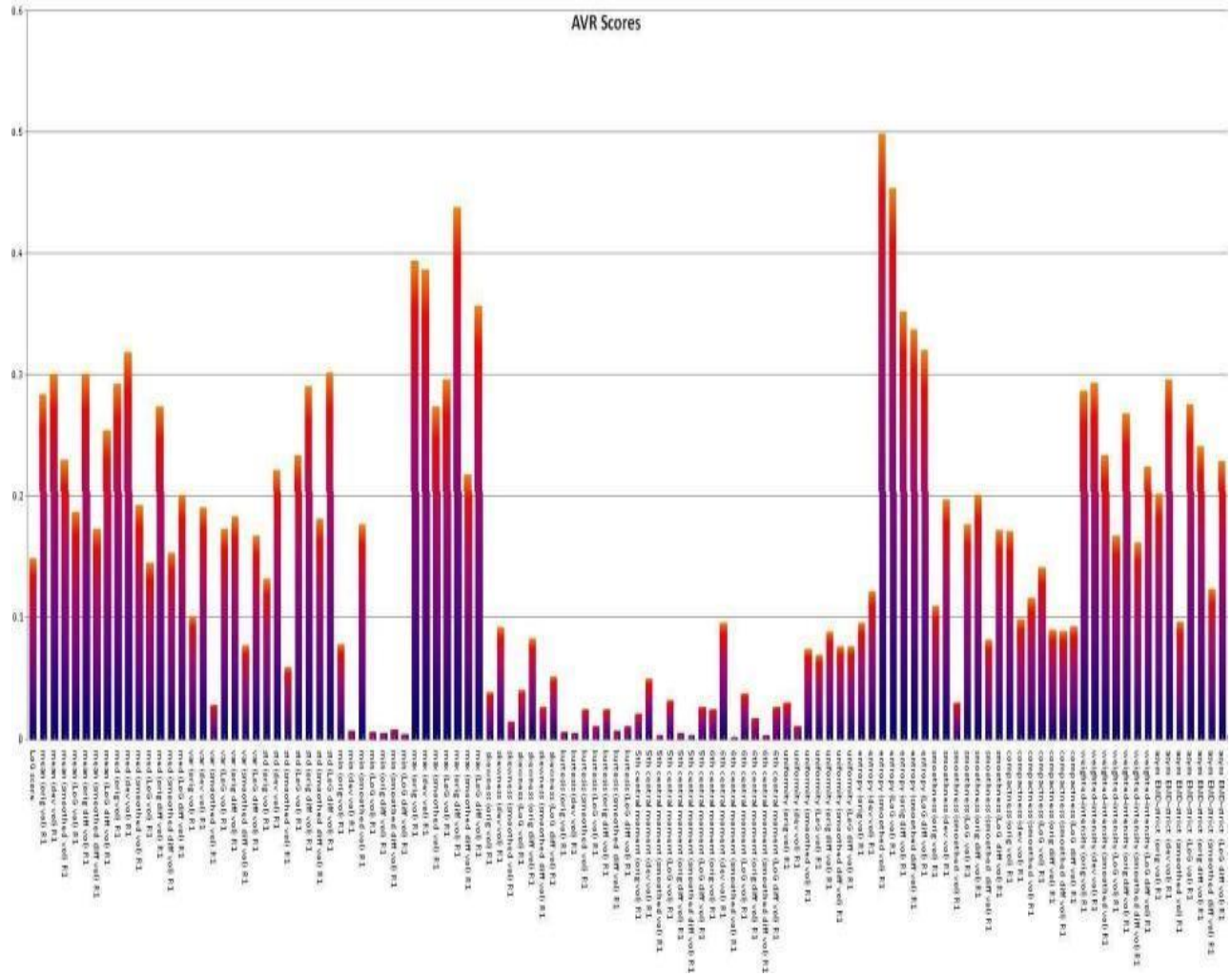

ROC Curves for All Features

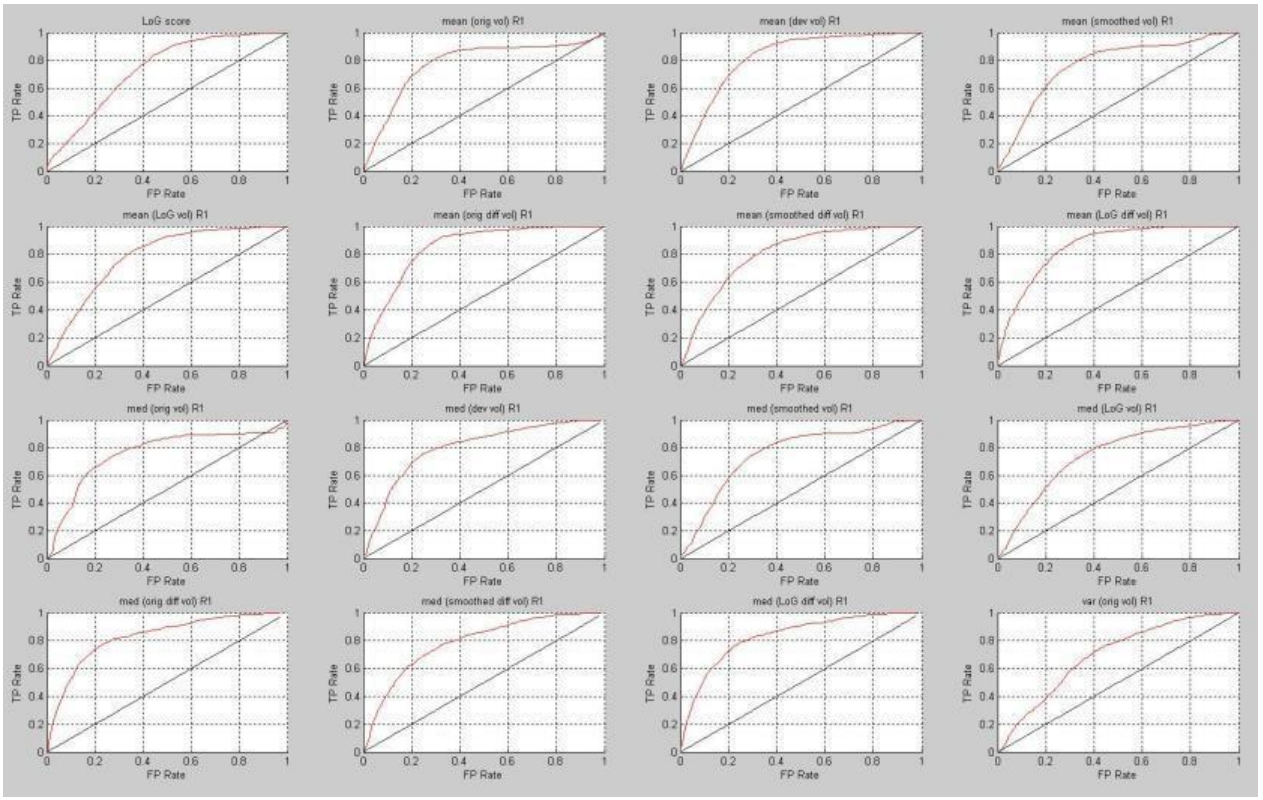

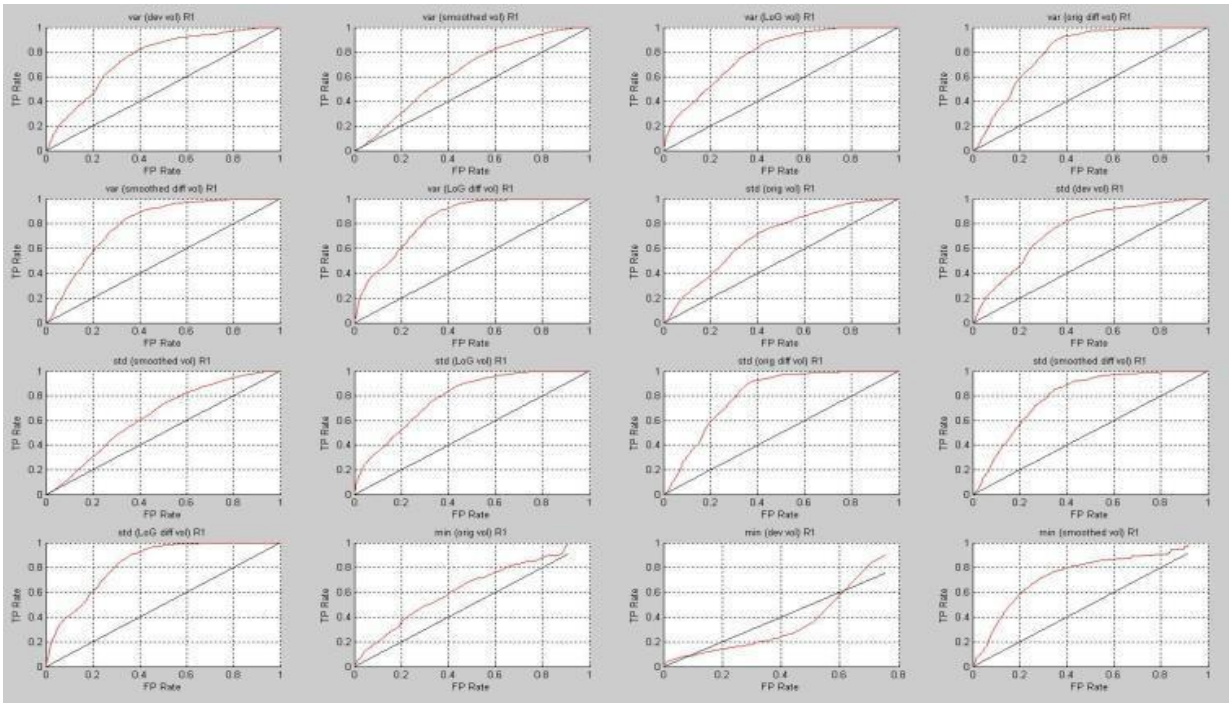

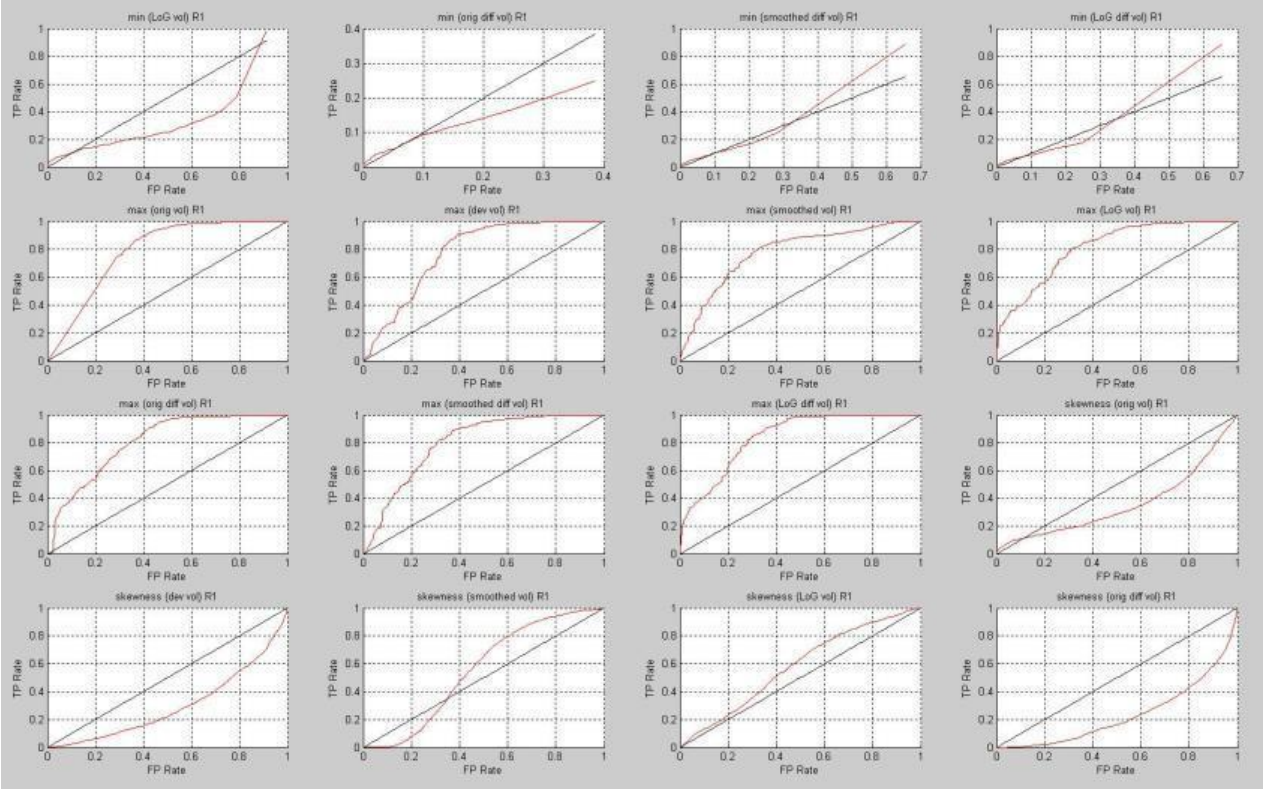
min (LoG vol) R1
min (orig diff vol) R1
min (smoothed diff vol) R1
min (LoG diff vol) R1
max (orig vol) R1
max (dev vol) R1
max (smoothed vol) R1
max (LoG vol) R1
max (orig diff vol) R1
max (smoothed diff vol) R1
max (LoG diff vol) R1
skewness (orig vol) R1
skewness (dev vol) R1
skewness (smoothed vol) R1
skewness (LoG vol) R1
skewness (orig diff vol) R1
TP Rate
FP Rate

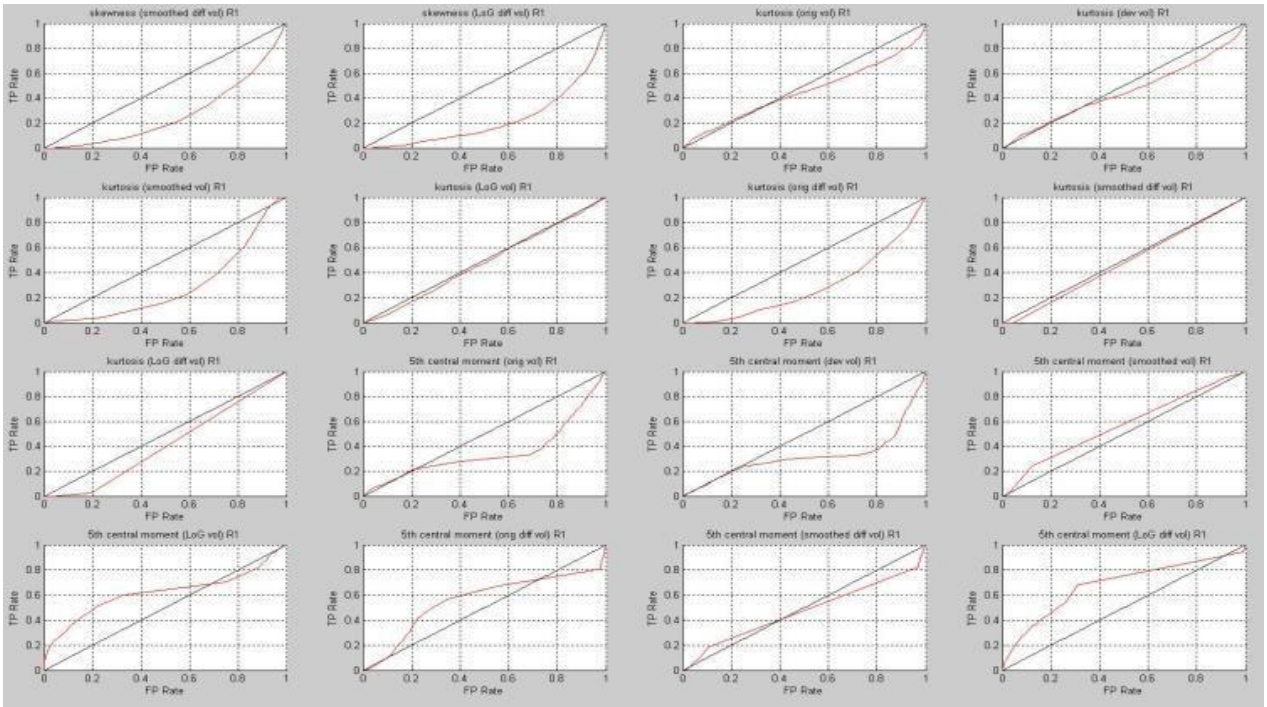
skewness (smoothed diff vol) R1
skewness (LoG diff vol) R1
kurtosis (orig vol) R1
kurtosis (dev vol) R1
kurtosis (smoothed vol) R1
kurtosis (LoG vol) R1
kurtosis (orig diff vol) R1
kurtosis (smoothed diff vol) R1
kurtosis (LoG diff vol) R1
5th central moment (orig vol) R1
5th central moment (dev vol) R1
5th central moment (smoothed vol) R1
5th central moment (LoG vol) R1
5th central moment (orig diff vol) R1
5th central moment (smoothed diff vol) R1
5th central moment (LoG diff vol) R1
TP Rate
FP Rate

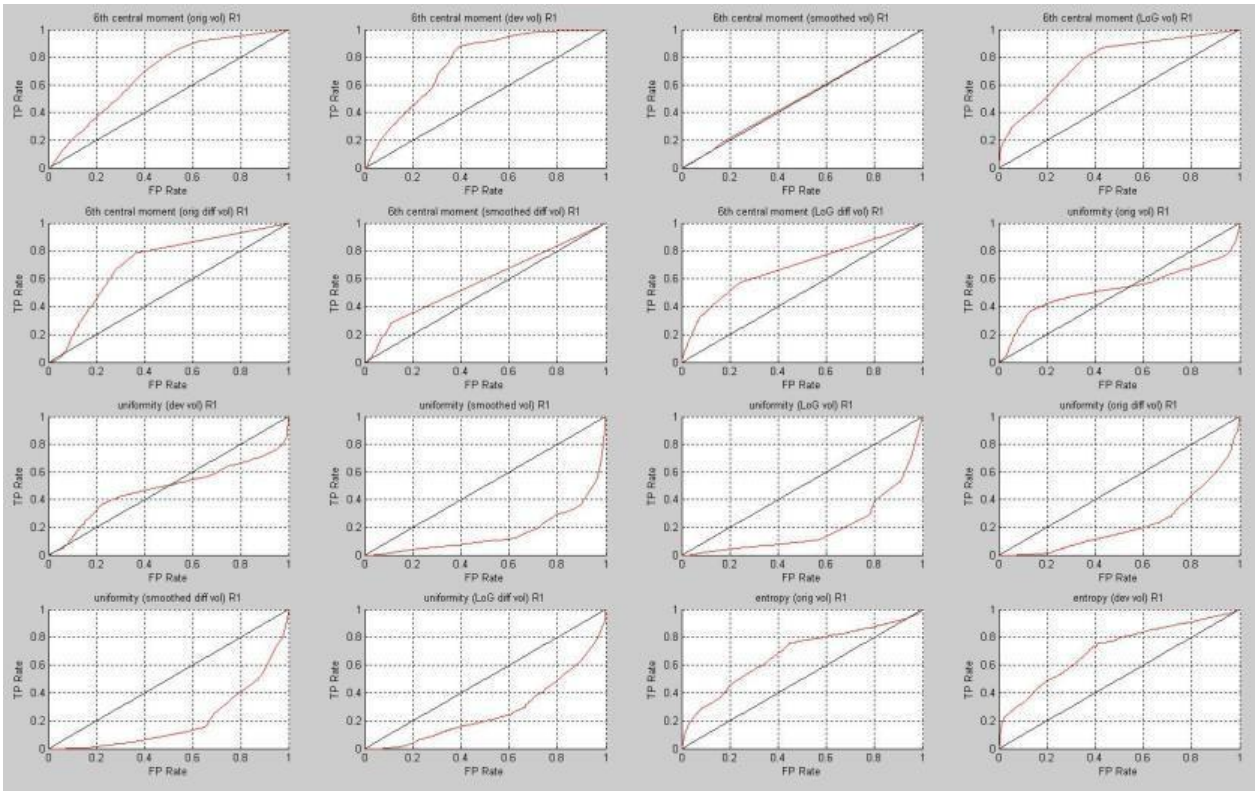
6th central moment (orig vol) R1
6th central moment (dev vol) R1
6th central moment (smoothed vol) R1
6th central moment (LoG vol) R1
6th central moment (orig diff vol) R1
6th central moment (smoothed diff vol) R1
6th central moment (LoG diff vol) R1
uniformity (orig vol) R1
uniformity (dev vol) R1
uniformity (smoothed vol) R1
uniformity (LoG vol) R1
uniformity (orig diff vol) R1
uniformity (smoothed diff vol) R1
uniformity (LoG diff vol) R1
entropy (orig vol) R1
entropy (dev vol) R1
TP Rate
FP Rate

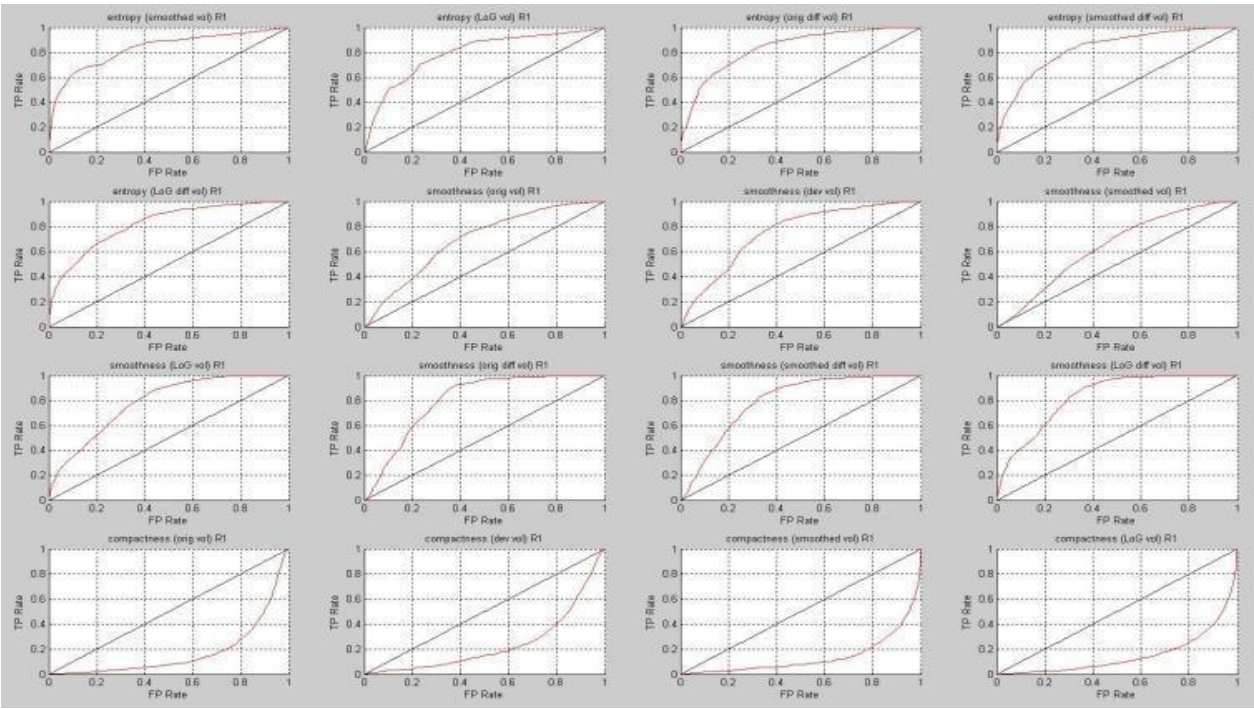
entropy (smoothed vol) R1
entropy (LoG vol) R1
entropy (orig diff vol) R1
entropy (smoothed diff vol) R1
entropy (LoG diff vol) R1
smoothness (orig vol) R1
smoothness (dev vol) R1
smoothness (smoothed vol) R1
smoothness (LoG vol) R1
smoothness (orig diff vol) R1
smoothness (smoothed diff vol) R1
smoothness (LoG diff vol) R1
compactness (orig vol) R1
compactness (dev vol) R1
compactness (smoothed vol) R1
compactness (LoG vol) R1
TP Rate
FP Rate

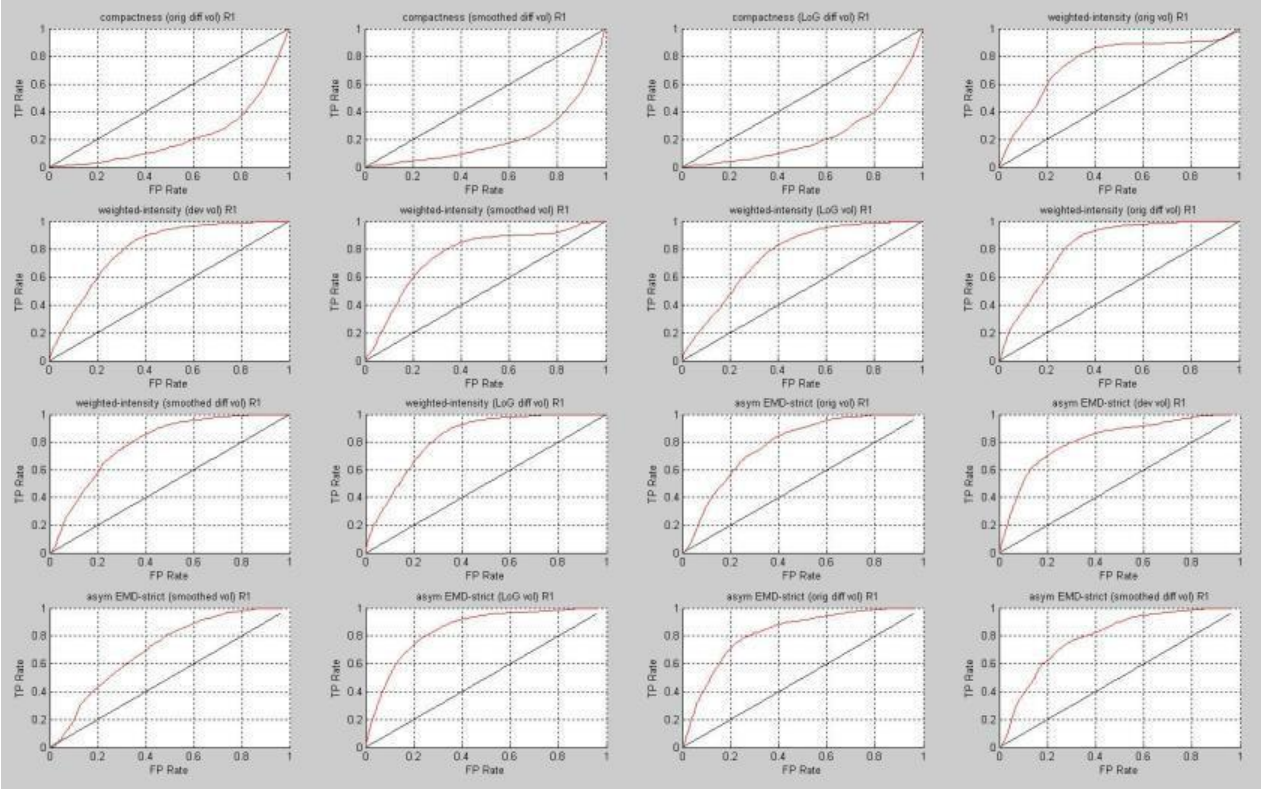
compactness (orig diff vol) R1
compactness (smoothed diff vol) R1
compactness (LoG diff vol) R1
weighted-intensity (orig vol) R1
weighted-intensity (dev vol) R1
weighted-intensity (smoothed vol) R1
weighted-intensity (LoG vol) R1
weighted-intensity (orig diff vol) R1
weighted-intensity (smoothed diff vol) R1
weighted-intensity (LoG diff vol) R1
asym EMD-strict (orig vol) R1
asym EMD-strict (dev vol) R1
asym EMD-strict (smoothed vol) R1
asym EMD-strict (LoG vol) R1
asym EMD-strict (orig diff vol) R1
asym EMD-strict (smoothed diff vol) R1
TP Rate
FP Rate

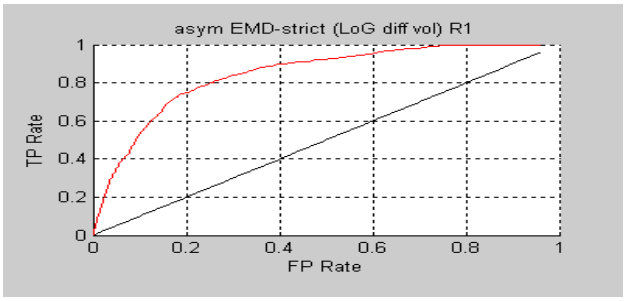
asym EMD-strict (LoG diff vol) R1
TP Rate
FP Rate

CHAPTER – 6 (ii)

Charts and Tables - Using My Ground Truth

A. No Asymmetry Features - SFS with QDA

Classifier	Tumor (Sensitivity)		Non-Tumor (Specificity)		Overall	
	Training	Test	Training	Test	Training	Test
Mahalanobis	85.7(+-0.4)	85.0(+-1.5)	87.6(+-0.6)	86.4(+-0.5)	86.7(+-0.4)	86.3(+-0.5)
Bayes(Lin)	85.6(+-0.5)	84.7(+-1.7)	88.0(+-0.4)	86.6(+-0.5)	86.8(+-0.3)	86.6(+-0.5)
Bayes(Quad)	85.6(+-0.5)	84.8(+-1.7)	87.9(+-0.4)	86.6(+-0.5)	86.8(+-0.3)	86.5(+-0.4)
LDA	85.6(+-0.5)	84.7(+-1.7)	88.0(+-0.4)	86.6(+-0.5)	86.8(+-0.3)	86.6(+-0.5)
QDA	85.6(+-0.5)	84.8(+-1.7)	87.9(+-0.4)	86.6(+-0.5)	86.8(+-0.3)	86.5(+-0.4)
SVM (linear)	79.2(+-0.8)	78.9(+-1.2)	84.0(+-1.4)	83.9(+-1.4)	81.6(+-0.8)	83.8(+-1.3)

confusion matrix
Training set : Total Tumors :**1354** ; Total Non-Tumors :**1354** ;
Test set : Total Tumors :**338** ; Total Non-Tumors :**27482**;

TT (True Positive)		TN (False Positive)		NT (False Negative)		NN (True Negative)	
Training	Test	Training	Test	Training	Test	Training	Test
1161.2(+-6.0)	287.5(+-5.0)	167(+-9.0)	3736(+-150.3)	192.8(+-6.0)	50.5(+-5.0)	1187(+-9.0)	23746(+-150.3)
1159.3(+-8.0)	286.6(+-5.9)	162.4(+-6.1)	3660.1(+-153.6)	194.7(+-8.0)	51.4(+-5.9)	1191.6(+-6.1)	23821.9(+-153.6)
1160(+-7.5)	286.9(+-5.8)	163.1(+-6.1)	3677.2(+-142.1)	194(+-7.5)	51.1(+-5.8)	1190.9(+-6.1)	23804.8(+-142.1)
1159.3(+-8.0)	286.6(+-5.9)	162.4(+-6.1)	3660.1(+-153.6)	194.7(+-8.0)	51.4(+-5.9)	1191.6(+-6.1)	23821.9(+-153.6)
1160(+-7.5)	286.9(+-5.8)	163.1(+-6.1)	3677.2(+-142.1)	194(+-7.5)	51.1(+-5.8)	1190.9(+-6.1)	23804.8(+-142.1)
1073.1(+-11.0)	266.7(+-4.2)	216.4(+-19.5)	4423.2(+-391.1)	280.9(+-11.0)	71.3(+-4.2)	1137.6(+-19.5)	23058.8(+-391.1)

B. Only Asymmetry Features - SFS with QDA

Classifier	Tumor (Sensitivity)		Non-Tumor (Specificity)		Overall	
	Training	Test	Training	Test	Training	Test
Mahalanobis	81.4(+-0.7)	82.3(+-2.3)	84.4(+-0.7)	83.5(+-0.5)	82.9(+-0.5)	83.5(+-0.5)
Bayes(Lin)	79.9(+-0.7)	80.3(+-2.4)	87.1(+-0.7)	85.8(+-0.5)	83.5(+-0.4)	85.7(+-0.5)
Bayes(Quad)	79.8(+-0.7)	80.2(+-2.4)	87.3(+-0.6)	85.9(+-0.6)	83.6(+-0.4)	85.8(+-0.6)
LDA	79.9(+-0.7)	80.3(+-2.4)	87.1(+-0.7)	85.8(+-0.5)	83.5(+-0.4)	85.7(+-0.5)
QDA	79.8(+-0.7)	80.2(+-2.4)	87.3(+-0.6)	85.9(+-0.6)	83.6(+-0.4)	85.8(+-0.6)
SVM (linear)	74.5(+-1.2)	75.7(+-1.8)	85.0(+-0.8)	84.9(+-0.8)	79.7(+-0.4)	84.8(+-0.8)

confusion matrix
Training set : Total Tumors :**1354** ; Total Non-Tumors :**1354** ;
Test set : Total Tumors :**338** ; Total Non-Tumors :**27482**;

TT (True Positive)		TN (False Positive)		NT (False Negative)		NN (True Negative)	
Training	Test	Training	Test	Training	Test	Training	Test
1102.3(+-9.7)	278.5(+-8.1)	210.7(+-9.4)	4511.7(+-150.4)	251.7(+-9.7)	59.5(+-8.1)	1143.3(+-9.4)	22970.3(+-150.4)
1082.4(+-9.5)	271.7(+-8.1)	174.2(+-9.9)	3885.1(+-162.9)	271.6(+-9.5)	66.3(+-8.1)	1179.8(+-9.9)	23596.9(+-162.9)
1081.6(+-9.8)	271.4(+-8.2)	171.3(+-9.1)	3857(+-178.2)	272.4(+-9.8)	66.6(+-8.2)	1182.7(+-9.1)	23625(+-178.2)
1082.4(+-9.5)	271.7(+-8.1)	174.2(+-9.9)	3885.1(+-162.9)	271.6(+-9.5)	66.3(+-8.1)	1179.8(+-9.9)	23596.9(+-162.9)
1081.6(+-9.8)	271.4(+-8.2)	171.3(+-9.1)	3857(+-178.2)	272.4(+-9.8)	66.6(+-8.2)	1182.7(+-9.1)	23625(+-178.2)
1009(+-16.9)	256(+-6.3)	202.7(+-11.4)	4129.1(+-236.5)	345(+-16.9)	82(+-6.3)	1151.3(+-11.4)	23352.9(+-236.5)

C. All features - SFS with QDA

Classifier	Tumor (Sensitivity)		Non-Tumor (Specificity)		Overall	
	Training	Test	Training	Test	Training	Test
Mahalanobis	90.6(+-0.4)	89.9(+-2.5)	92.1(+-0.5)	90.4(+-0.3)	91.3(+-0.4)	90.3(+-0.3)
Bayes(Lin)	90.6(+-0.5)	90.0(+-2.2)	91.9(+-0.6)	90.3(+-0.4)	91.3(+-0.4)	90.3(+-0.4)
Bayes(Quad)	90.7(+-0.4)	90.0(+-2.3)	92.1(+-0.5)	90.3(+-0.3)	91.4(+-0.4)	90.3(+-0.3)
LDA	90.6(+-0.5)	90.0(+-2.2)	91.9(+-0.6)	90.3(+-0.4)	91.3(+-0.4)	90.3(+-0.4)
QDA	90.7(+-0.4)	90.0(+-2.3)	92.1(+-0.5)	90.3(+-0.3)	91.4(+-0.4)	90.3(+-0.3)
SVM (linear)	79.9(+-0.7)	81.6(+-2.6)	88.1(+-1.0)	88.1(+-0.7)	84.0(+-0.5)	88.0(+-0.7)

confusion matrix
Training set : Total Tumors :**1354** ; Total Non-Tumors :**1354** ;
Test set : Total Tumors :**338** ; Total Non-Tumors :**27482**;

TT (True Positive)		TN (False Positive)		NT (False Negative)		NN (True Negative)	
Training	Test	Training	Test	Training	Test	Training	Test
1227.3(+-6.4)	304(+-8.4)	106.6(+-7.7)	2637(+-98.1)	126.7(+-6.4)	34(+-8.4)	1247.4(+-7.7)	24845(+-98.1)
1227.5(+-7.6)	304.4(+-7.6)	108.4(+-8.2)	2658.8(+-130.4)	126.5(+-7.6)	33.6(+-7.6)	1245.6(+-8.2)	24823.2(+-130.4)
1228.2(+-6.7)	304.3(+-8.0)	106.6(+-7.7)	2647(+-105.6)	125.8(+-6.7)	33.7(+-8.0)	1247.4(+-7.7)	24835(+-105.6)
1227.5(+-7.6)	304.4(+-7.6)	108.4(+-8.2)	2658.8(+-130.4)	126.5(+-7.6)	33.6(+-7.6)	1245.6(+-8.2)	24823.2(+-130.4)
1228.2(+-6.7)	304.3(+-8.0)	106.6(+-7.7)	2647(+-105.6)	125.8(+-6.7)	33.7(+-8.0)	1247.4(+-7.7)	24835(+-105.6)
1082.9(+-10.7)	275.9(+-8.7)	160.3(+-14.1)	3256.1(+-211.4)	271.1(+-10.7)	62.1(+-8.7)	1193.7(+-14.1)	24225.9(+-211.4)

CHAPTER – 7

Ground Truth - Major Differences

Case : Chen Ping's vs. Mine

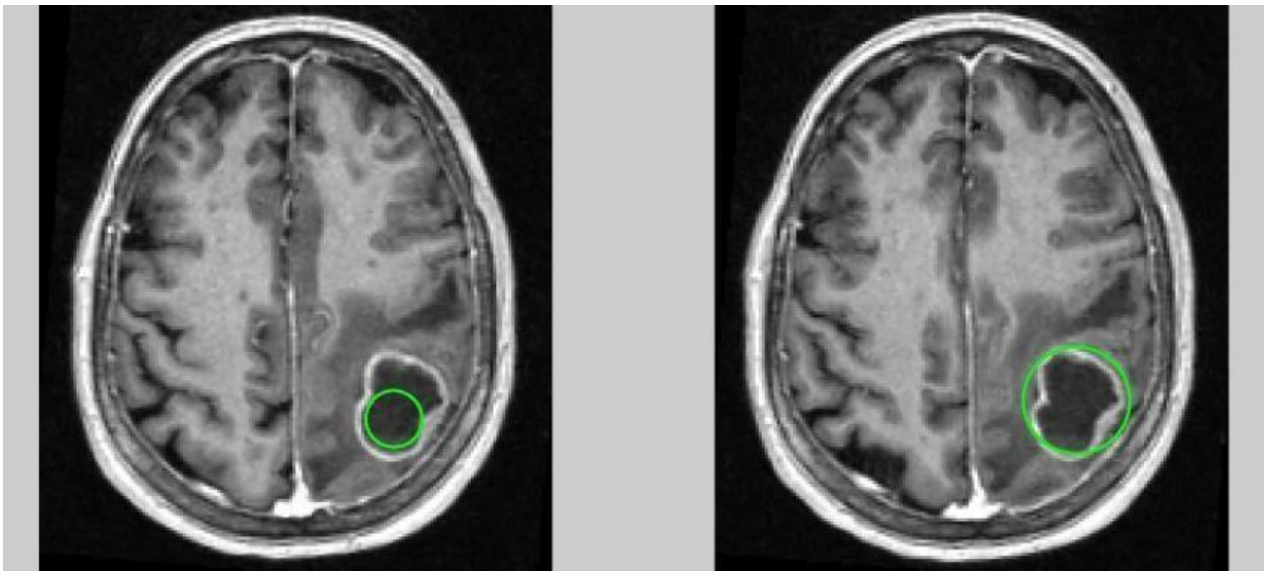

Case : Chen Ping's vs. Mine

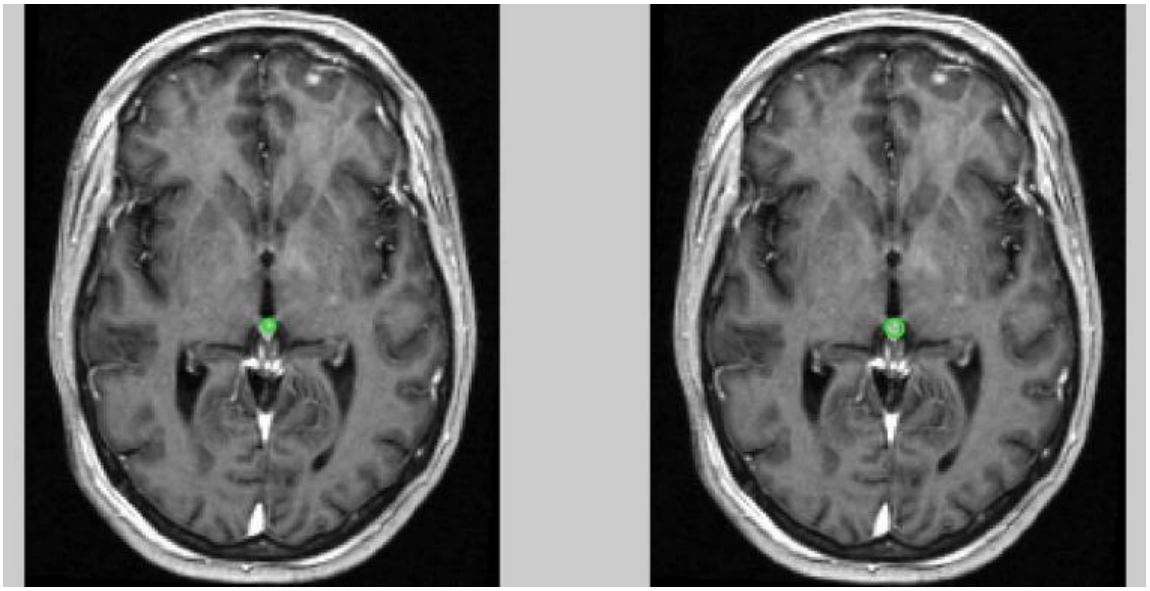

Case : Chen Ping's vs. Mine

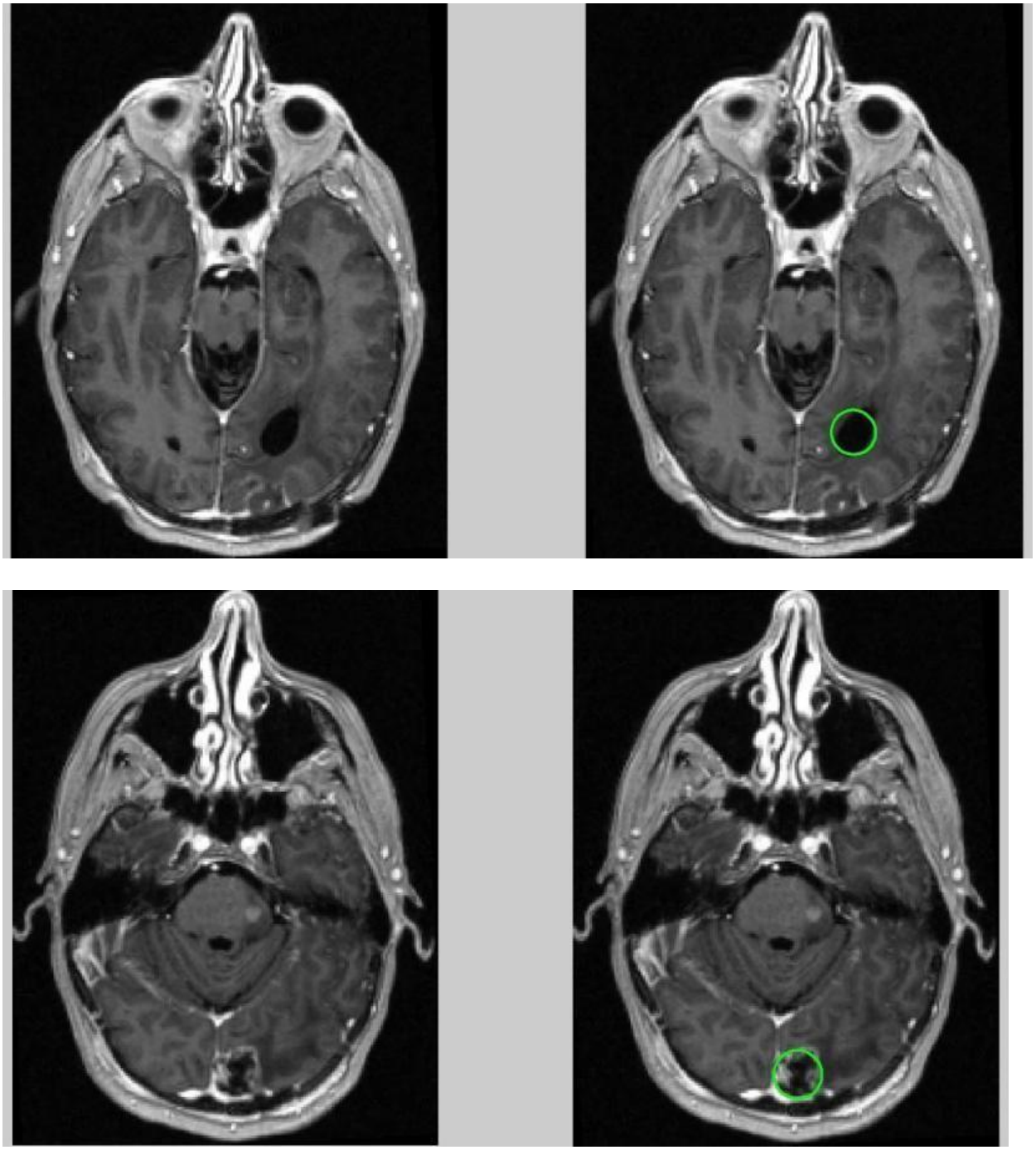

Case : Chen Ping's vs. Mine

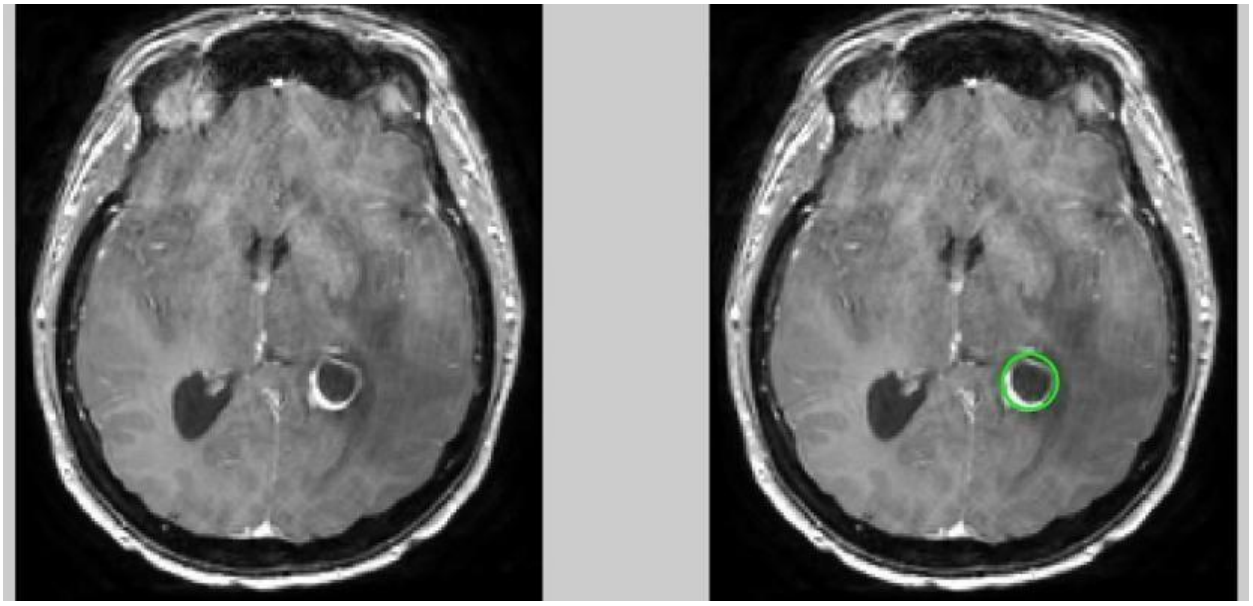

Case : Chen Ping's vs. Mine

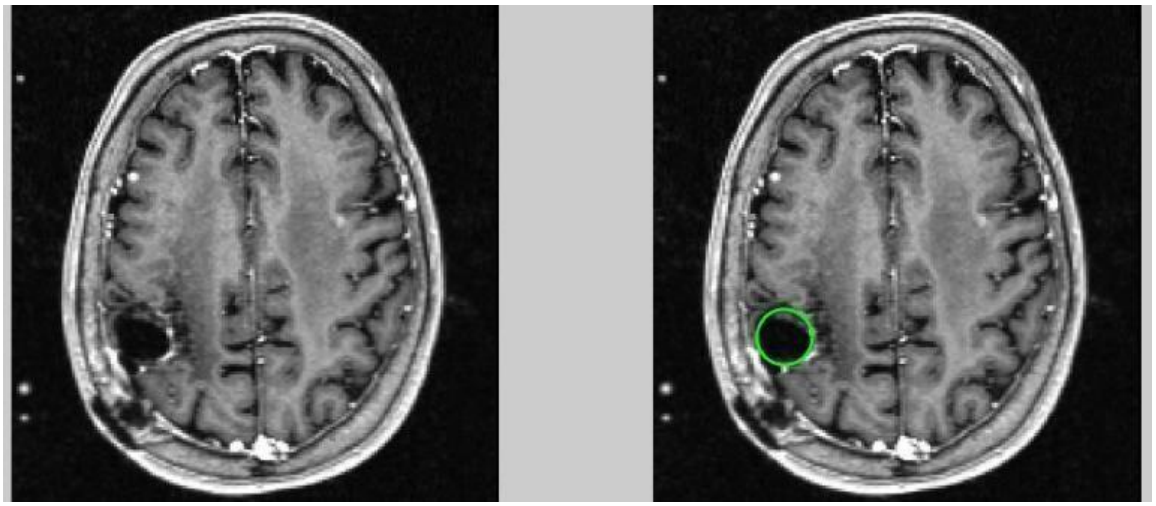

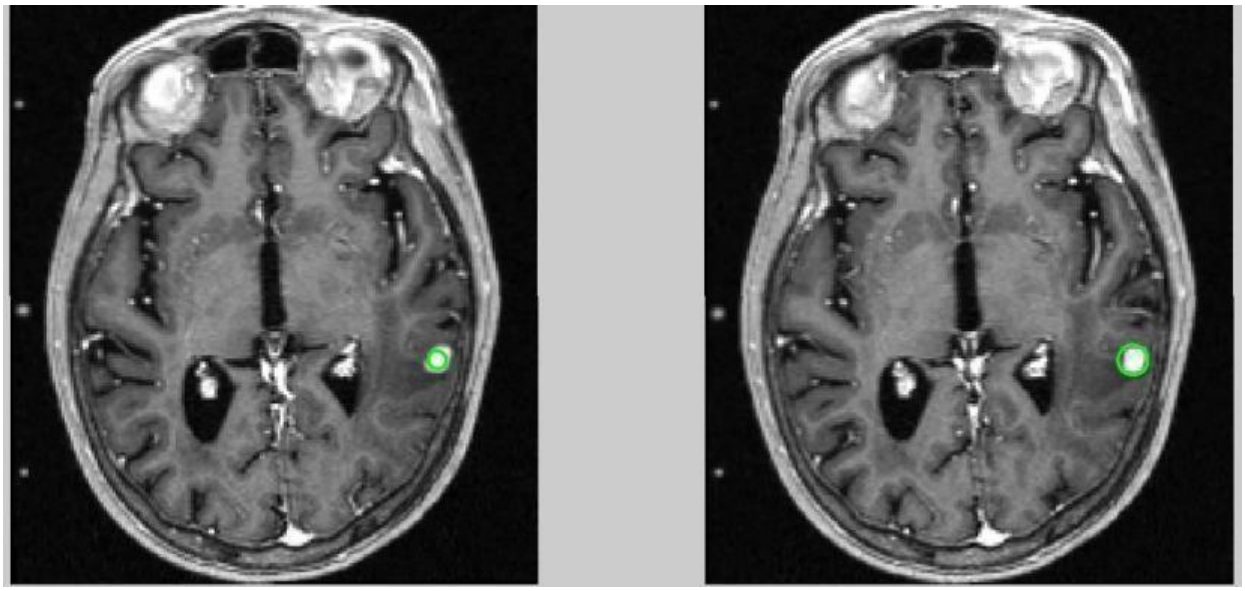

Case : Chen Ping's vs. Mine

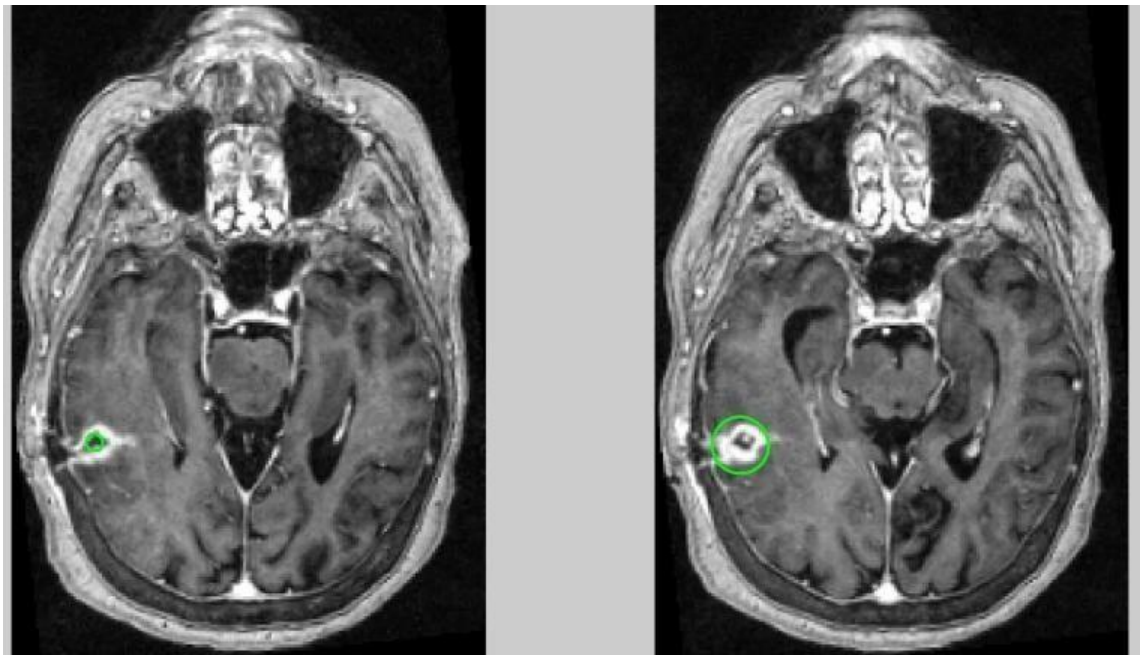

Case : Chen Ping's vs.Mine

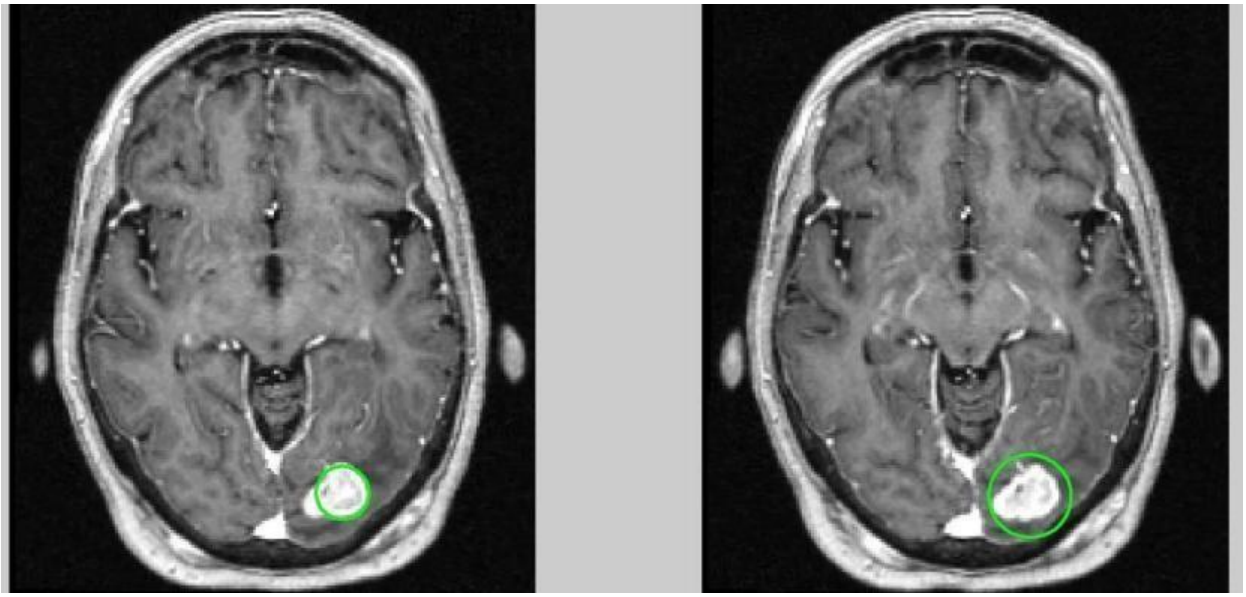

Case : Chen Ping's vs.Mine

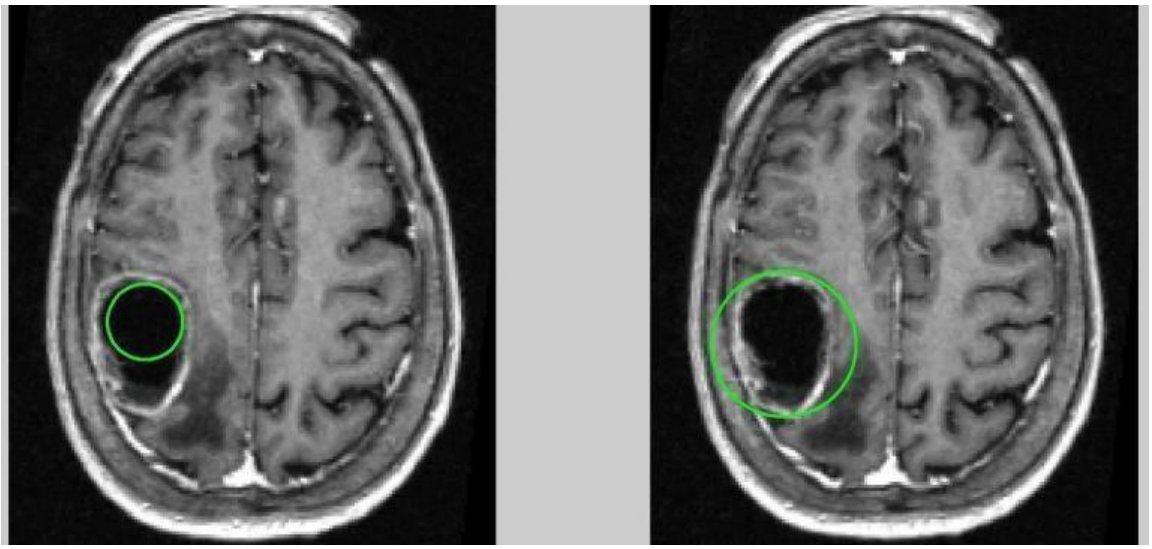

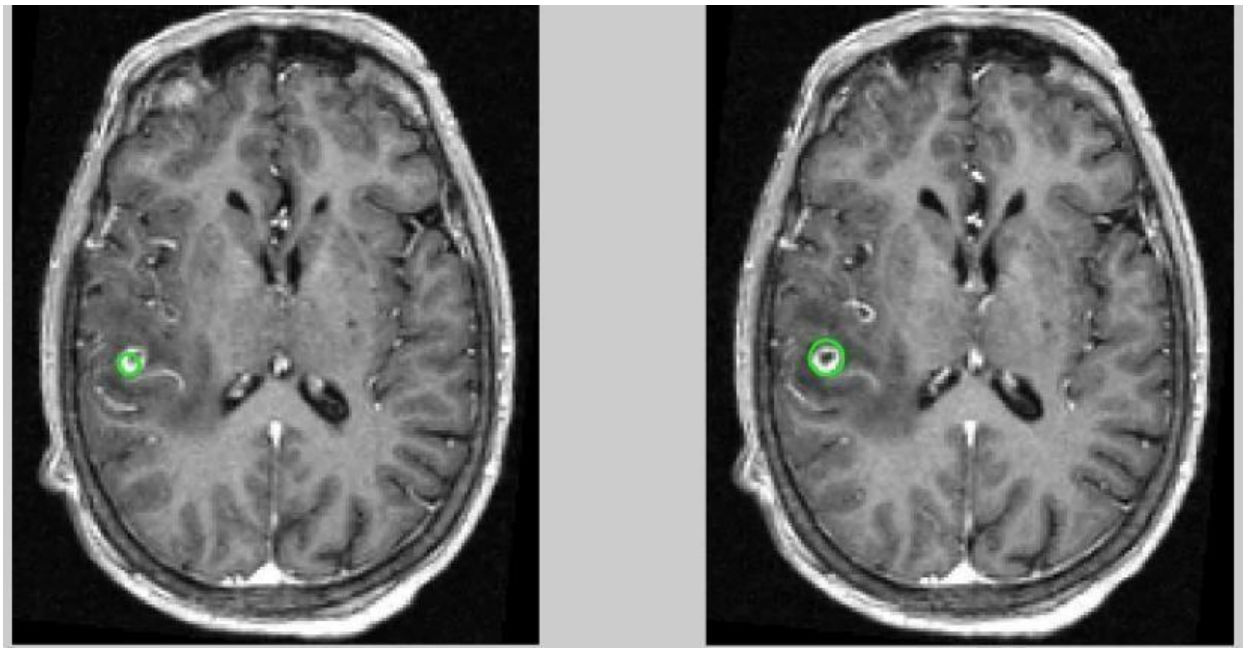

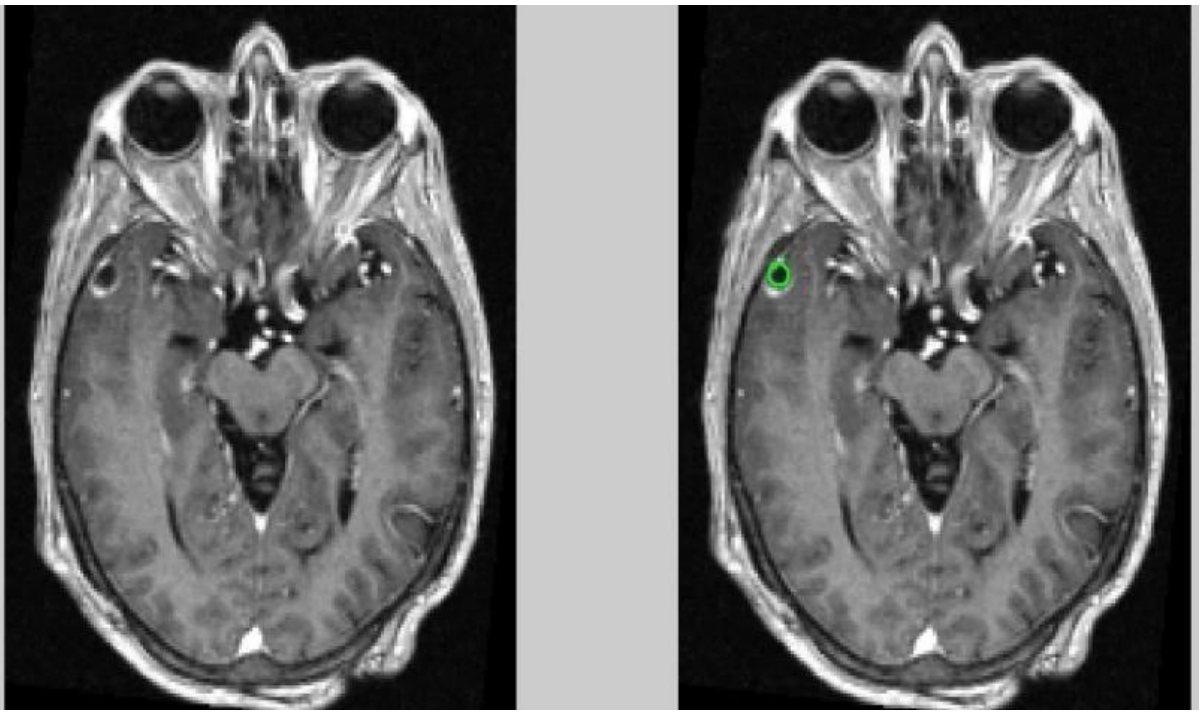

Case : Chen Ping's vs. Mine

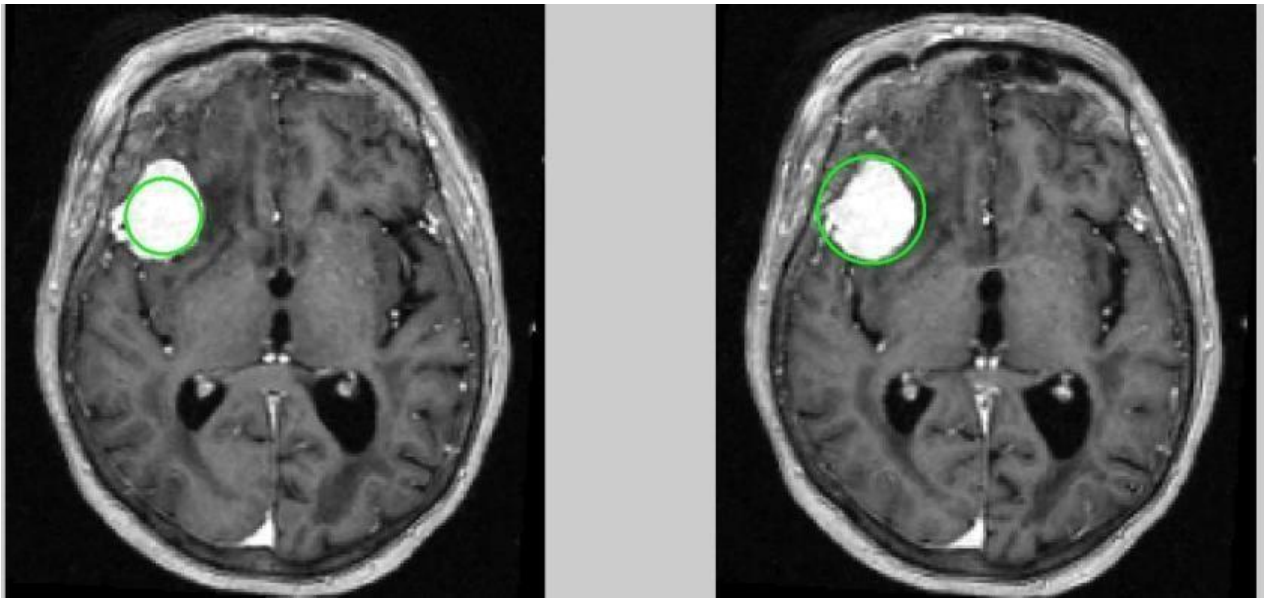

Case : Chen Ping's vs. Mine

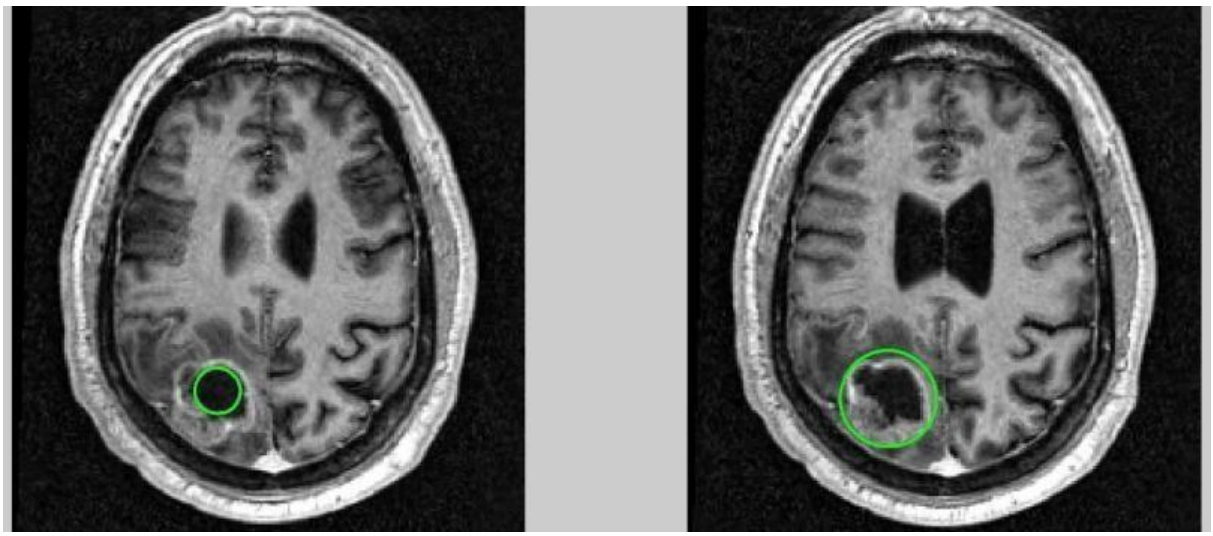

Case : Chen Ping's vs. Mine

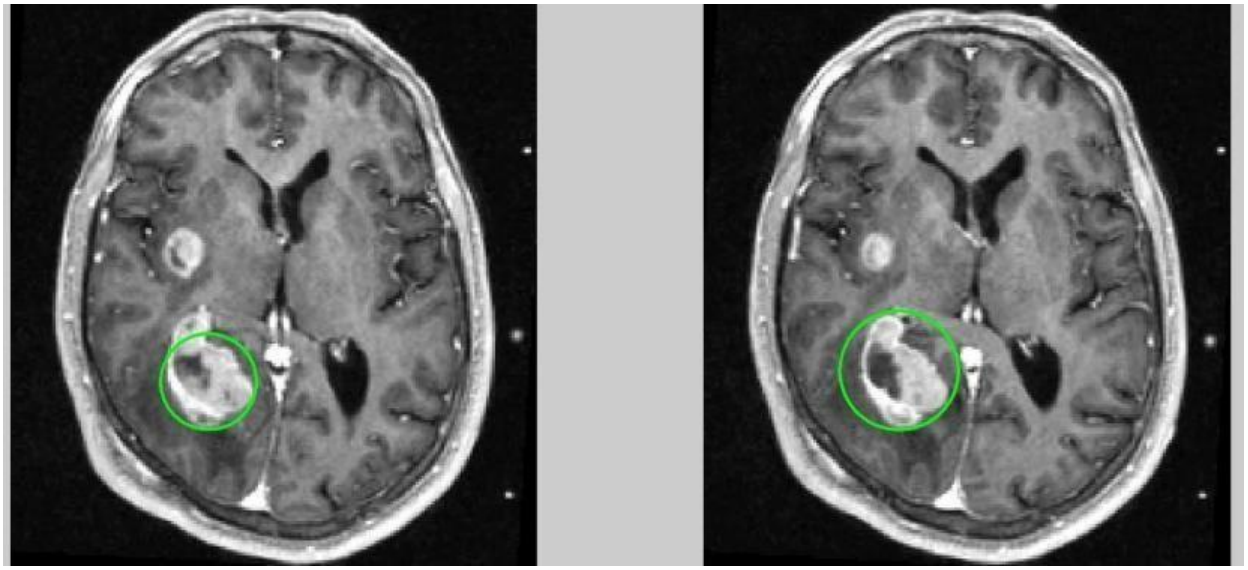

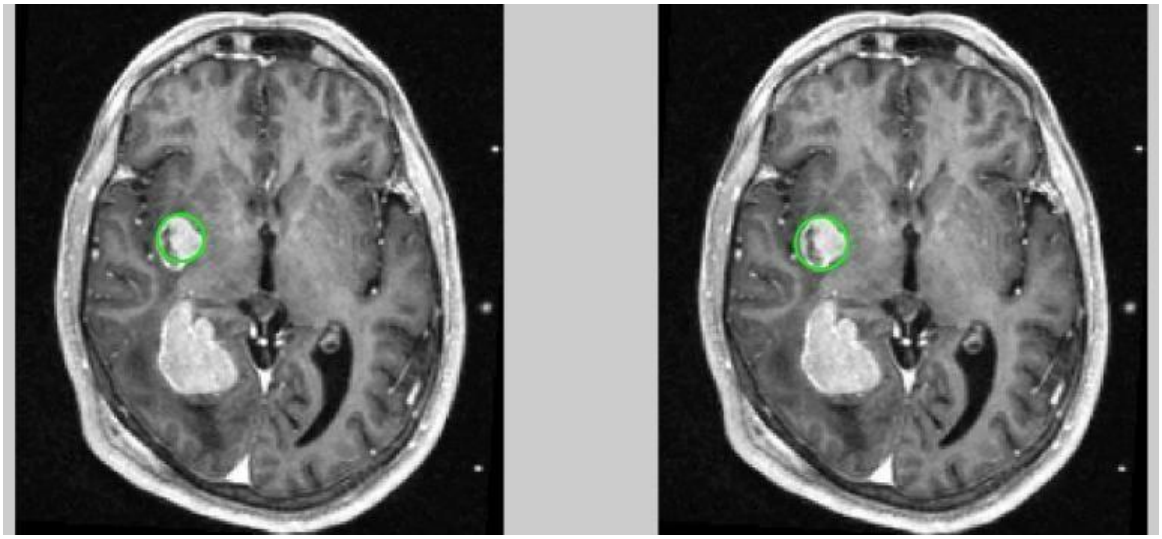

Case : Chen Ping's vs. Mine

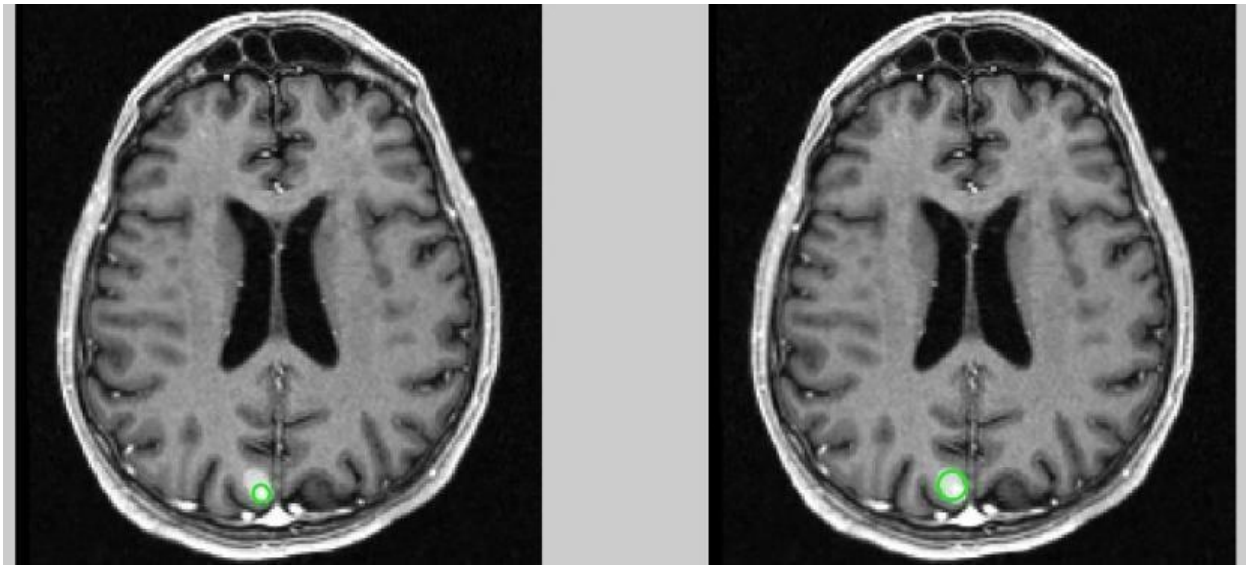

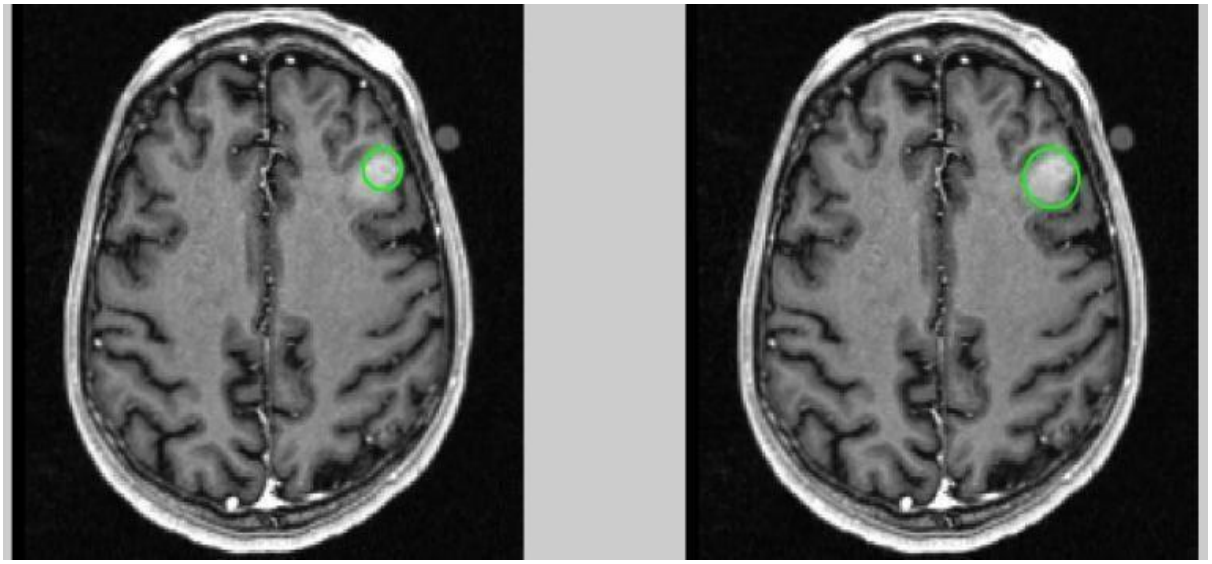

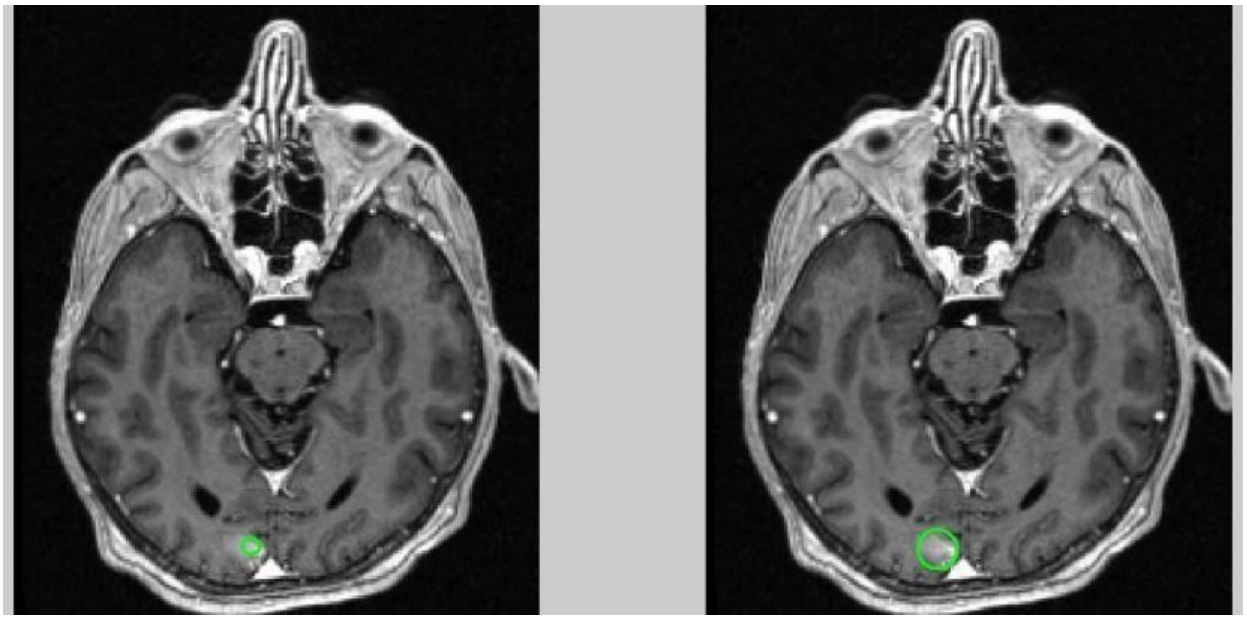

Case : Chen Ping's vs. Mine

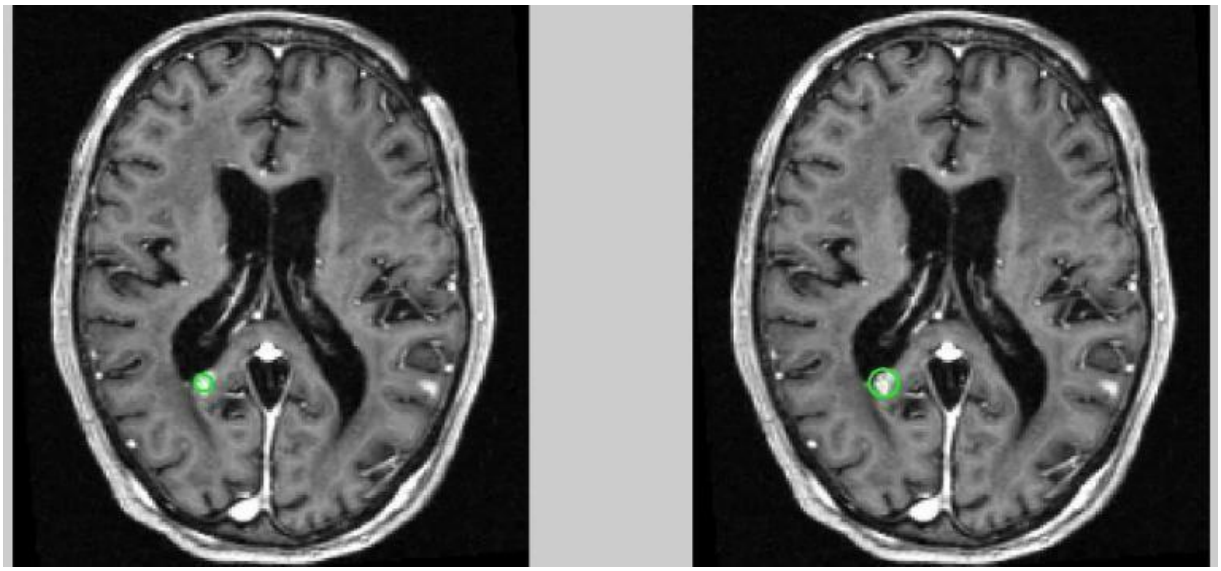

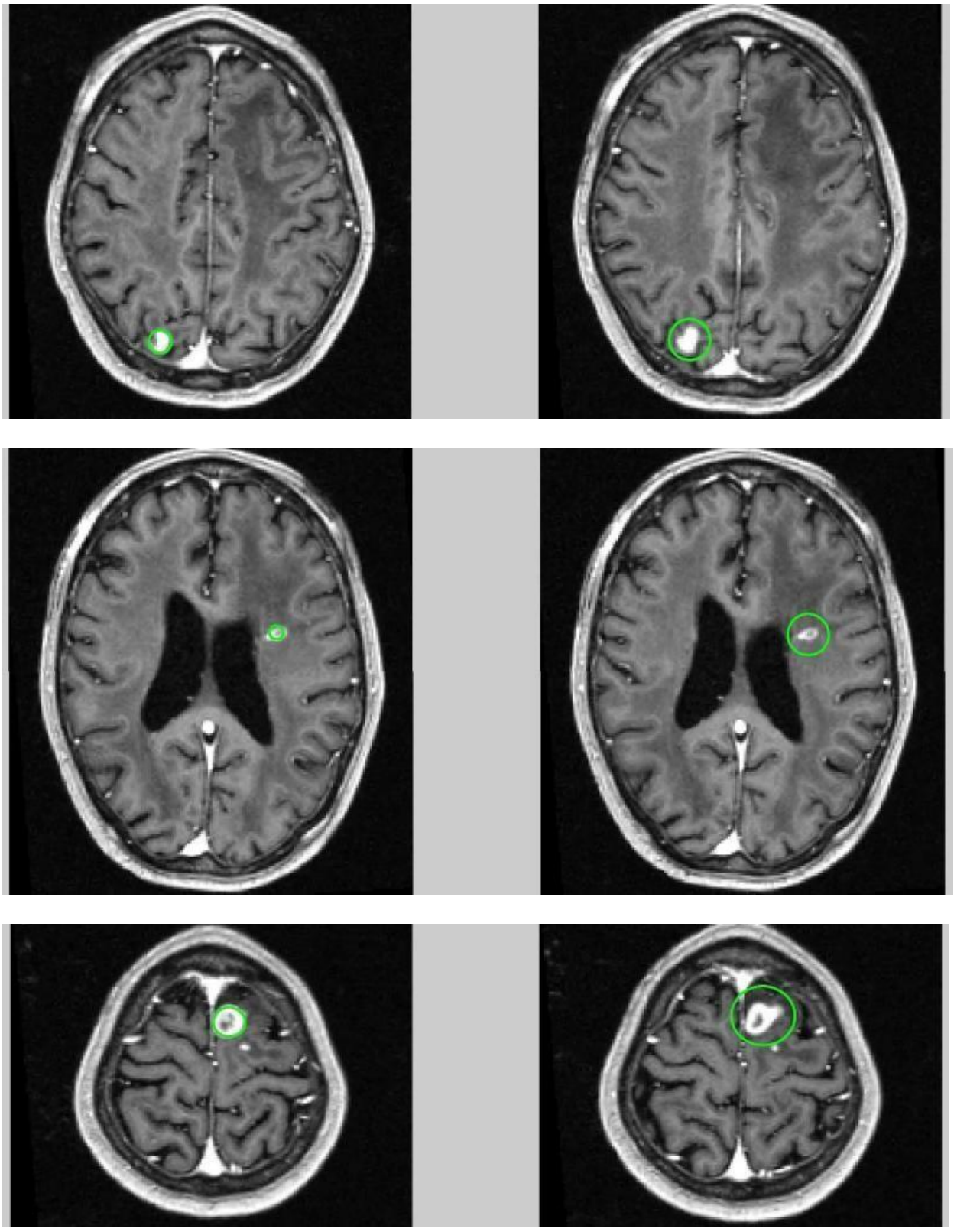

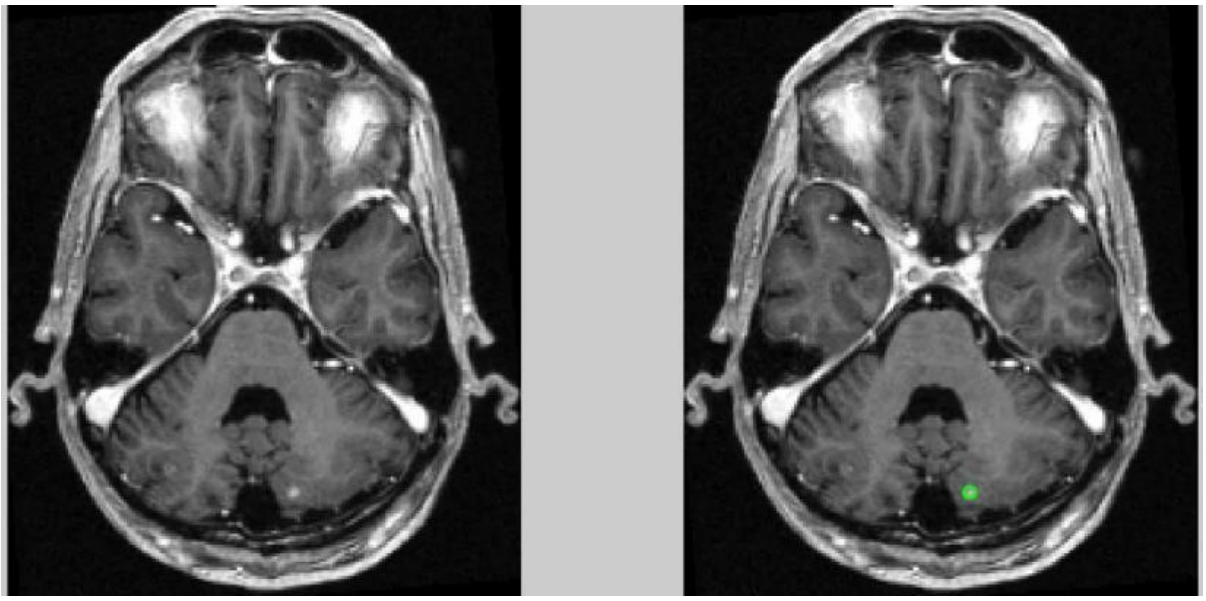

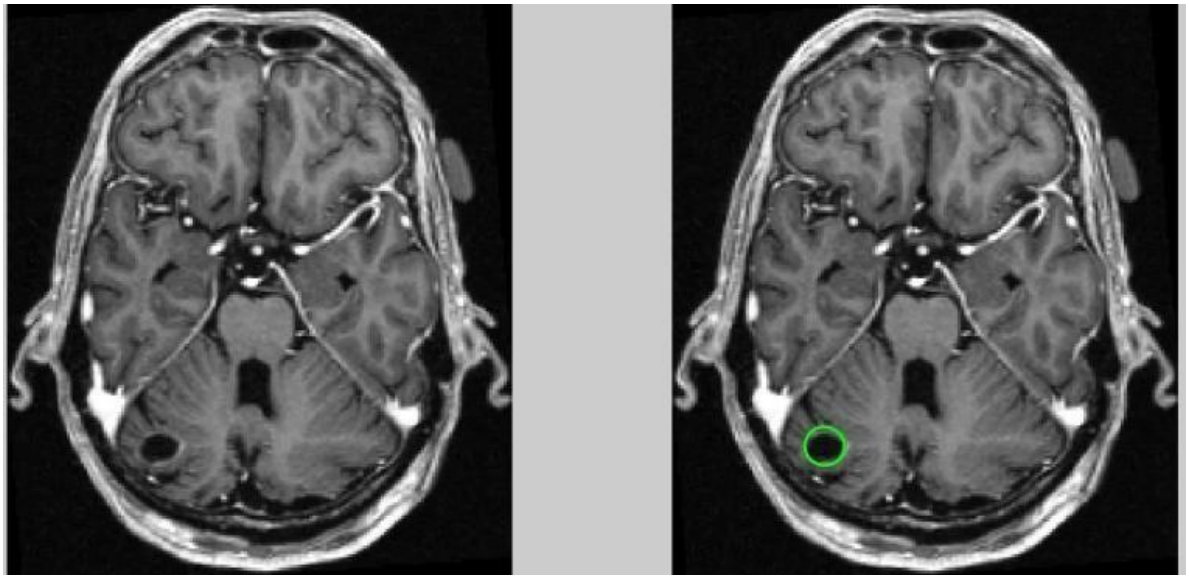

Case : Chen Ping's vs. Mine

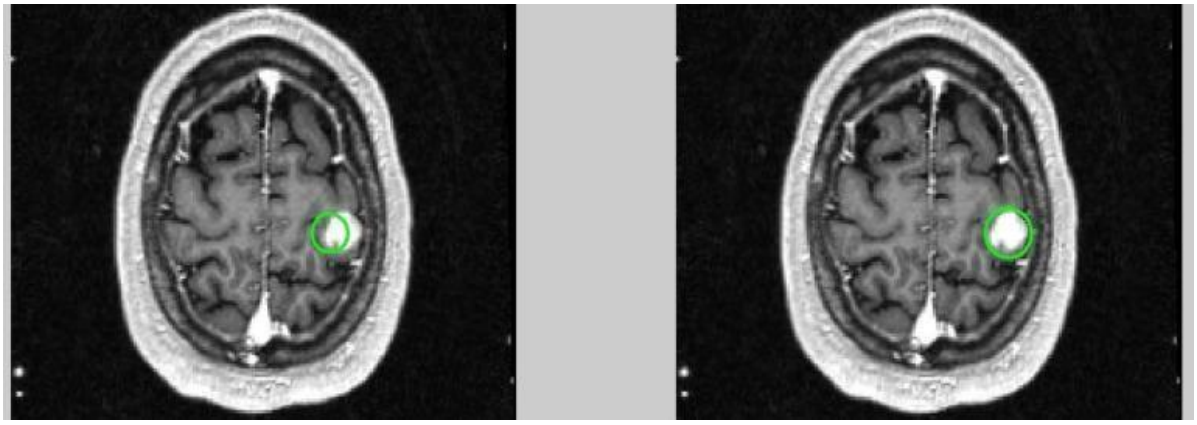

CHAPTER - 8

CONCLUSION

As per the literature survey, all the implemented model shows the good accuracy in classifying the benign tumor the accuracy drops while classifying the malignant tumor. In our proposed method, a better accuracy is obtained in classifying the malignant tumor (accuracy of 99%) comparing to the other existing system. The proposed method is limited that classifies the tumor as benign, malignant or normal, in future enhancement we are going to implement the algorithm that can also be able to classify the grade of the tumor.

CHAPTER - 9
FUTURE SCOPE

The robustness in terms of speed makes such computer assisted systems a positive contributor in medical diagnostics. DL approaches are beneficial in brain tumor research by aiding in automatic feature acquisitions. This overcomes the consumption of time as compared to manual engineering of features. The advent of GPUs makes the computation processes very fast. In addition, performance increases with increase of training data. Apart from such advantages, some limitations are also observed by using DL approaches in brain tumor domain. The high cost of GPUs makes the DL process very costly. Also, no detailed literature is found to help in the selection of specific deep network architecture for particular brain analysis problem. This study will provide hint to the researchers in observing that what recent DL models are employed in brain analysis so that further research can be performed by keeping in view the existing DL .

CHAPTER - 10

REFERENCES

1. J. Amin, M. Sharif, M. Raza, and M. Yasmin, "Detection of Brain Tumor based on Features Fusion and Machine Learning," Journal of Ambient Intelligence and Humanized Computing, pp. 1-17, 2018.

2. J. Amin, M. Sharif, M. Raza, T. Saba, and M. A. Anjum, "Brain tumor detection using statistical and machine learning method," Computer methods and programs in biomedicine, vol. 177, pp. 69-79, 2019.

3. J. Amin, M. Sharif, M. Yasmin, T. Saba, and M. Raza, "Use of machine intelligence to conduct analysis of human brain data for detection of abnormalities in its cognitive functions," Multimedia Tools and Applications, pp. 1-19, 2019.

4. J. H. Shah, Z. Chen, M. Sharif, M. Yasmin, and S. L. Fernandes, "A novel biomechanics-based approach for person re-identification by generating dense color sift salience features," Journal of Mechanics in Medicine and Biology, vol. 17, p. 1740011, 2017.

5. S. L. Fernandes, V. P. Gurupur, N. R. Sunder, N. Arunkumar, and S. Kadry, "A novel nonintrusive decision support approach for heart rate measurement," Pattern Recognition Letters, 2017.